Electronic Supplementary Material (ESI) for Chemical Science.

Supplementary Information for:

Electrification of a Milstein-type Catalyst for Alcohol Reformation

Damien Tocqueville[a], Francesco Crisanti[a], Julian Guerrero[a], Esther Nubret[a], Marc Robert[a,b] ,David Milstein[c] and Niklas von Wolff*[a]

[a.] *Laboratoire d'Electrochimie Moléculaire*
Université Paris Cité, CNRS
F-75006 Paris, France.
[b.] *Institut Universitaire de France (IUF),*
F-75005 Paris, France.
[c.] *Department of Molecular Chemistry and Materials Science, The Weizmann Institute of Science*
Rehovot 7610001, Israel.

1. General

All manipulations unless stated otherwise were performed using Schlenk or glovebox techniques under dry argon or nitrogen atmosphere, respectively. THF was dried over Na/benzophenone, freshly distilled prior to use and stored under nitrogen atmosphere over molecular sieves (4Å). 1,2-Difluorobenzene (DFB) was degassed and dried over activated molecular sieves (4Å). $NaPF_6$ was recrystallized from acetonitrile and dried under high vacuum prior to use. $(TBA)PF_6$ was recrystallized from ethanol and dried under high vacuum prior to use. Anhydrous deuterated solvents were purchased from Eurisotop and stored over 4Å molecular sieves. All chemicals unless noted otherwise were purchased from major commercial suppliers (TCI, Sigma-Aldrich) and used as received. NMR spectra were measured on a Bruker Avance II 400 MHz spectrometer. The following abbreviations are used for describing NMR spectra: s (singlet), d (doublet), t (triplet), td (triplet of doublets), ddd (doublet of doublets of doublets), vd (virtual doublet), vt (virual triplet), br (broad). CV and CPE experiments were carried out using an AUTOLAB potentiostat (Metrohm) with a three-electrode set-up in a home-made cell (3 mL).

2. Cyclic voltammetry (CV) studies

2.1. General

CVs were run in a 3 mL cell with a 3-electrode set-up comprising of a Pt-wire counter electrode, a glassy carbon (GC) working electrode (1 or 3 mm diameter) and a reference electrode (leak-free Ag/AgCl or activated carbon paste electrode)[1] under N_2 or Ar atmosphere. Potentials are referenced with respect to a ferrocene solution in the same electrolyte and measured before and after a set of CV experiments to confirm the absence of potential drift. The GC-working electrode is washed, polished with diamond paste (0.25 µm particle size) and rinsed with acetone and ultrapure water (>18.2 MΩ cm–1, Millipore Milli-Q), after which it was sonicated for 2 mins in acetone, rinsed with ultrapure water and acetone and dried before use. The Pt-wire counter electrode is washed with acetone and ultrapure water, followed by flame-annealing prior to use. The reference electrode is separated from the solution by a porous glass frit. Ohmic drop is measured and compensated for all CVs using the positive feedback iR-compensation implemented in the Metrohm Nova 2.1.4 software.

2.2. DOSY-NMR and number of electrons transferred

In order to solve the Randles–Sevcik equation, to confirm the diffusive nature of the species involved and to determine the number of electorns transferred, the diffusion coefficient of **1** needs to be measured (using DOSY-NMR). In 0.5 mL of *d₈*-THF, 6.5 mM of **1** were mixed with 0.2 M $NaPF_6$. A ^{1}H-NMR was recorded to confirm stability of **1**. Diffusion coefficients were calculated based on the aromatic pyridine protons. From two resonances at 7.72 and 7.32 a mean diffusion coefficient of 8.54×10^{-10} m^2/s (8.54×10^{-6} cm^2/s) was derived. Using the Randles–Sevcik equation (1), the number of electrons transferred (2) can be derived by plotting the peak current versus the square root of the scan rate (see manuscript, Figure 1):

$$i_p = 0.4463\, nFAC\left(\frac{nFvD}{RT}\right)^{\frac{1}{2}} \quad (1)$$

$$n = \frac{m^{\frac{2}{3}}(RT)^{\frac{1}{3}}}{FA^{\frac{2}{3}}C^{\frac{2}{3}}D^{\frac{1}{3}}} \quad (2),$$

Where F is the Faradaic constant, A the surface area of the electrode, C the initial catalyst concentration, *v* the scan rate, *D* the diffusion coefficient obtained from DOSY-NMR, R the gas constant, T the temperature and *m* the slope of the *ip* vs $v^{1/2}$ curve. With *D* (8.54 x 10^{-6}) and *m* (3,577 x 10^{-5}) obtained experimentally, we observed $n = 0.94$ electrons transferred.

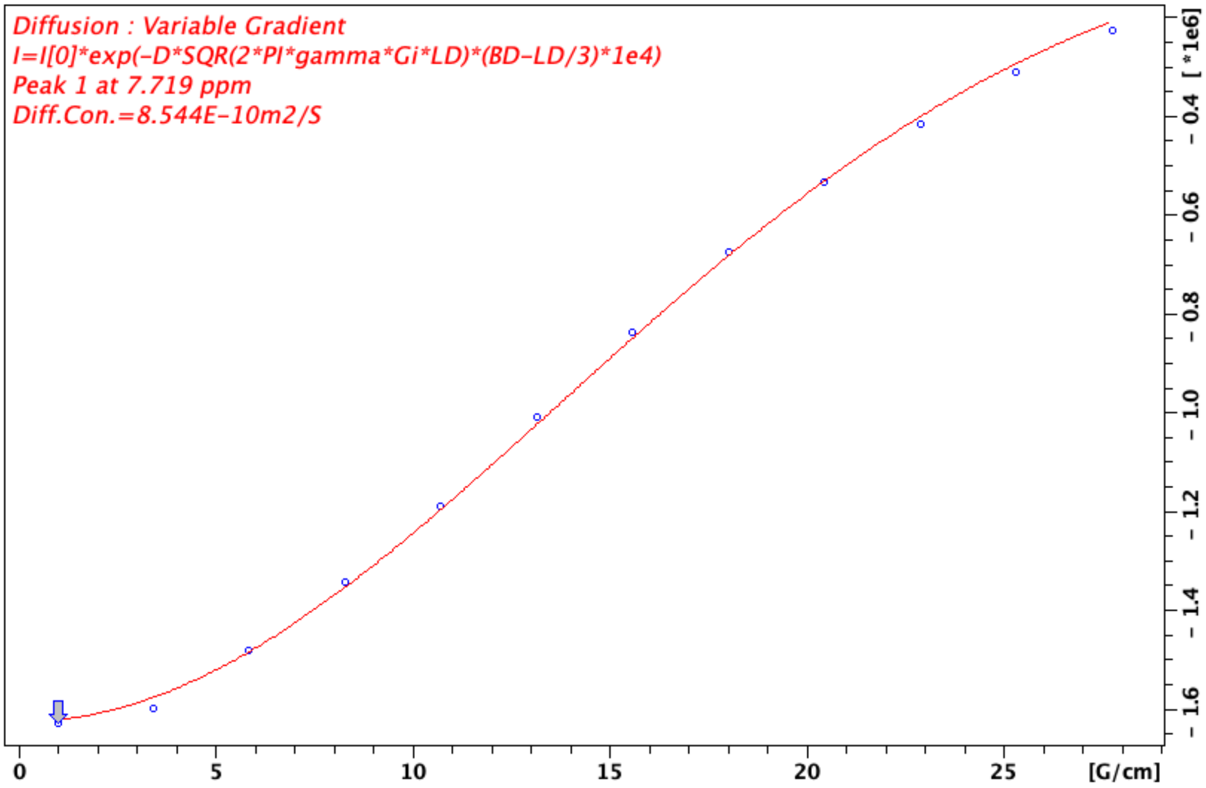

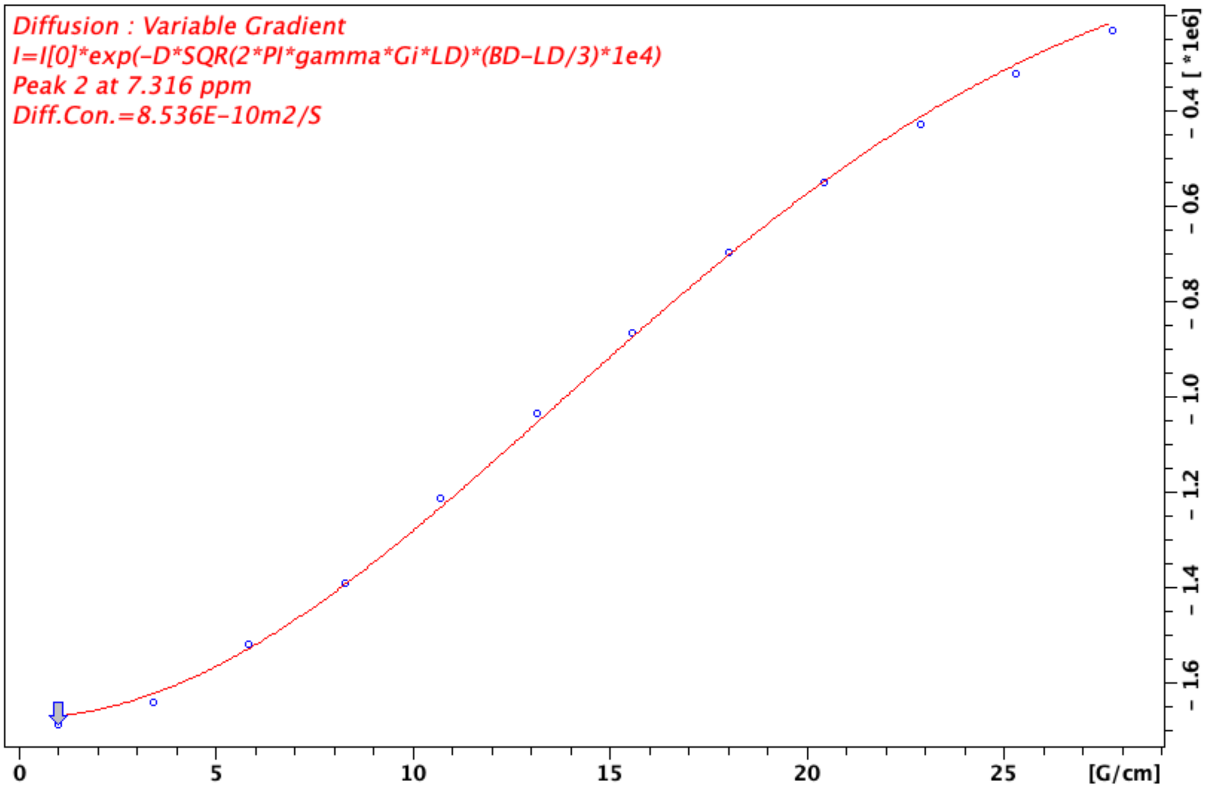

2.3. Dependance on catalyst concentration in 0.2M $NaPF_6$ in 2:1 THF/DFB

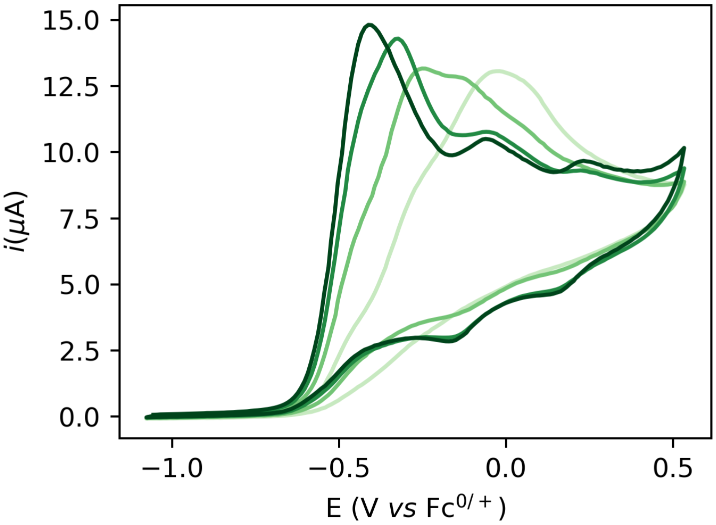

Figure SI1. CVs of a of **1** in 0.2M $NaPF_6$ in 2:1 THF/DFB in the presence of NaOEt (10 mM) and EtOH (200 mM) at different concentrations of **1** (from light to dark green: 0.5, 1, 1.5 and 2 mM of **1**).

2.4. In 0.1M $TBAPF_6$ in THF

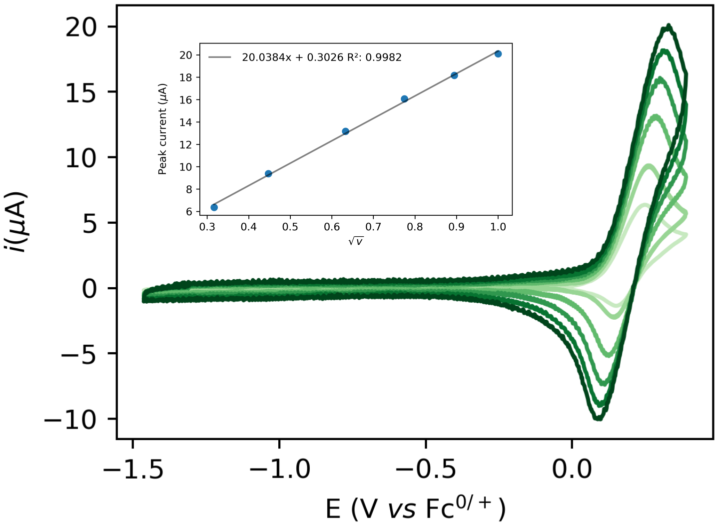

Figure SI2. CVs of a 2 mM solution of **1** in 0.1 M TBAPF$_6$ in THF at different scan rates (from light to dark green: 0.1, 0.2, 0.4, 0.6, 0.8 and 1.0 V/s). Inlet: evolution of the peak current with the square root of the scan rate.

2.5. In 0.1M TBAPF$_6$ in THF: low base concentration

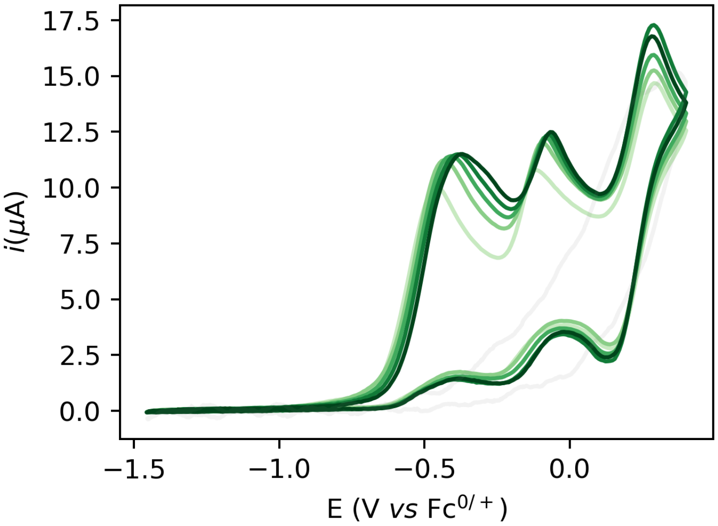

Figure SI3: Evolution of a 5 mM solution of **1** in 5 mM NaOEt, 0.2 M EtOH. (From light to dark green: 0.2, 0.4, 0.6, 0.8 and 1M EtOH, 0.1 V/s). Grey: in the absence of catalyst.

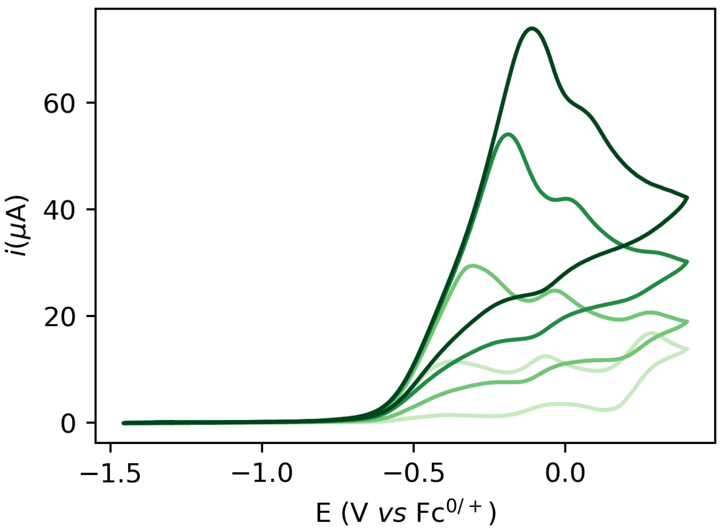

Figure SI4: Evolution of a 5 mM solution of **1** in 5 mM NaOEt, 1 M EtOH with base concentration. (From light to dark green: 5, 10, 15, and 20 mM NaOEt, 0.1 V/s)

2.6. In 0.1M TBAPF$_6$ in THF: high base concentration

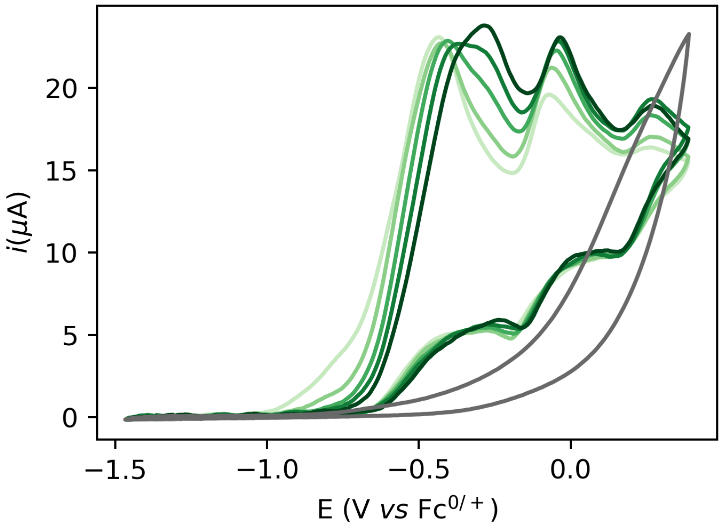

Figure SI5. CV of 200 mM EtOH, 10 mM NaOEt (grey) and in the presence of 5 mM **1** with increasing concentrations of EtOH (from light to dark green: 200, 400, 600, 800 and 1000mM; 0.1 V/s, 0.1M TBAPF$_6$). Grey: in the absence of catalyst.

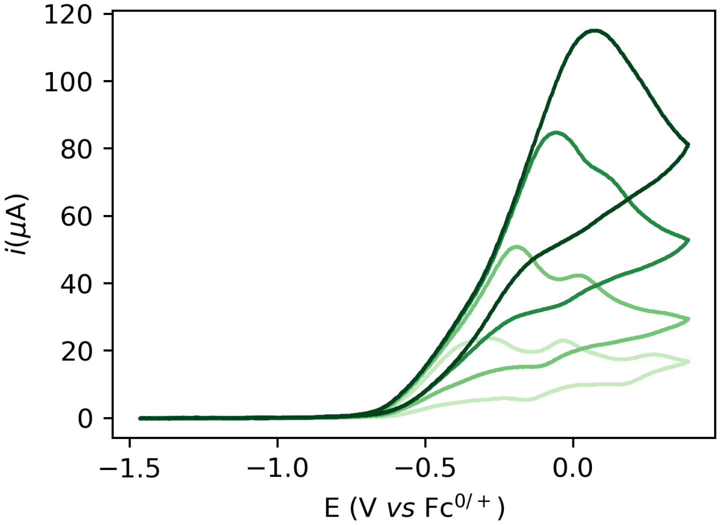

Figure SI6. CV of 5 mM **1**, 10 mM NaOEt, 1M EtOH with varying concentrations of base (10-40 mM NaOEt, light to dark green) in THF (0.1 V/s, 0.2 M $TBAPF_6$).

3. Synthesis and Electrochemical Characterization of 2, 3 and 4:

3.1. Characterization of 4 in 0.2 M $NaPF_6$ (2:1, THF/DFB)

In a J-Young NMR tube, to a solution of 6 mg (0.012 mmol) of **1** in 500 µL 1:1 THF/d_6-benzene were added 14 µL of sodium triethylborohydride (1 M in THF) and the tube was shaken vigorously (Glovebox). The reaction was monitored by ^{1}H- and ^{31}P{^{1}H}-NMR. After formation of **4** was confirmed by NMR, the mixture was filtrated over celite and added to roughly 1 mL of hexane for crystallization at -30°C. The hexane/crystal suspension was filtered over celite and washed with cold hexane (-30°C).

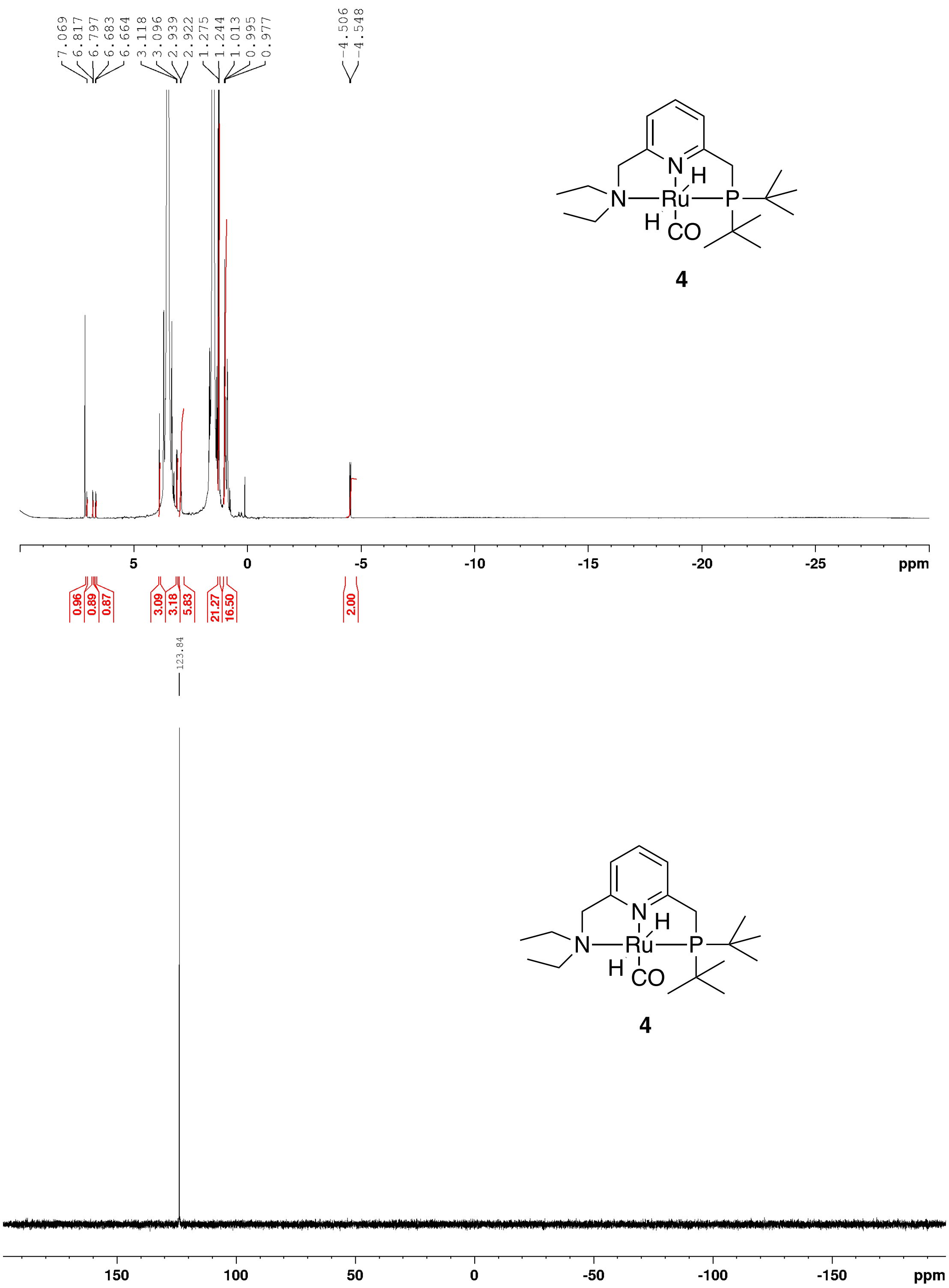

Figure SI7: ^{1}H (top) and $^{31}P\{^{1}H\}$ (bottom) NMR of **4** in 1:1 THF/d_6-benzene.

The yellow crystals were then extracted with 0.2 M $NaPF_6$ in 1:1 THF/d_6-benzene. The solution was added to an J-Young NMR tube and frozen immediately in liquid nitrogen. The evolution of **4** in the presence of $NaPF_6$ was then followed by low temperature ^{1}H- and ^{31}P-NMR.

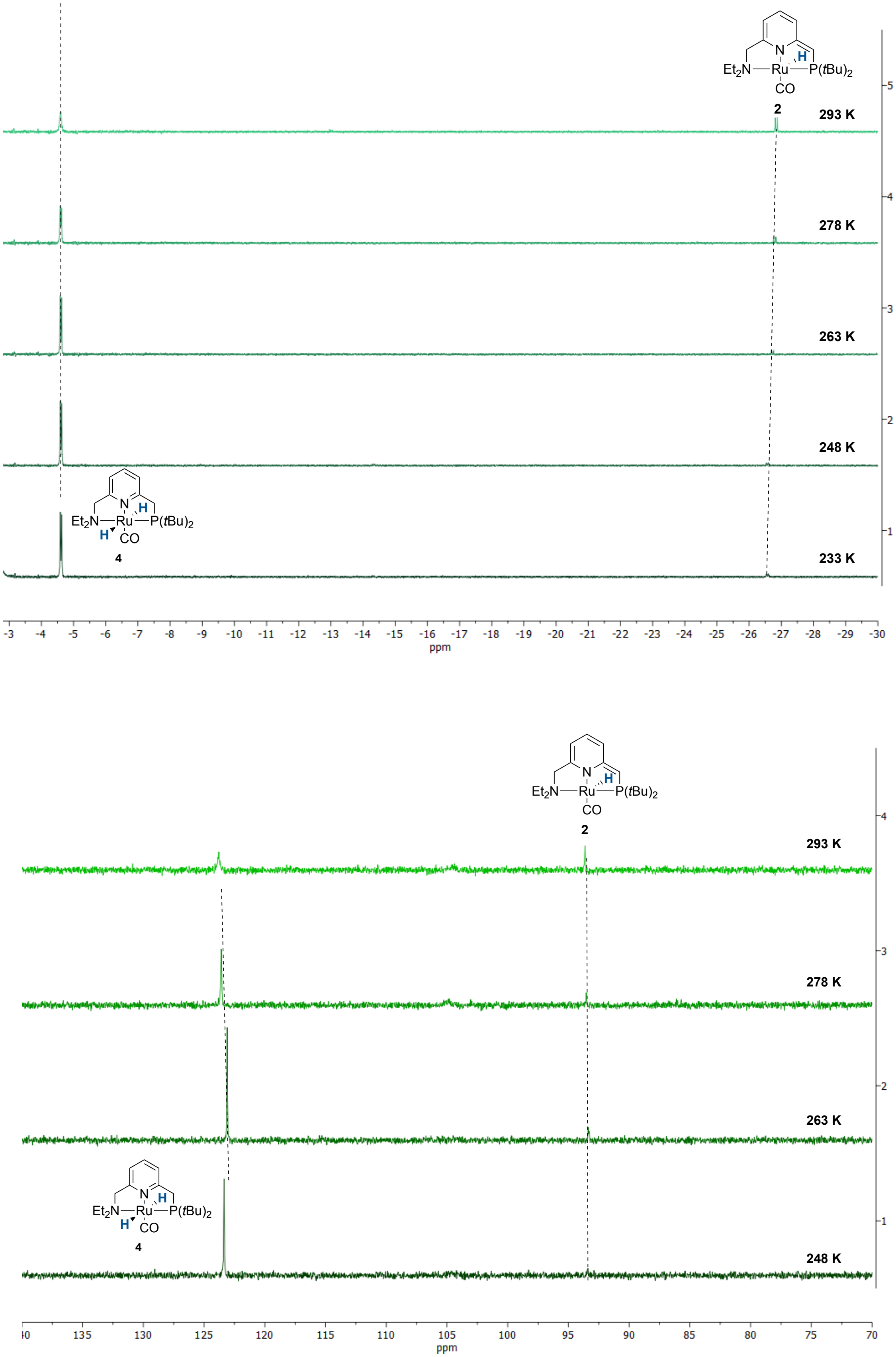

Figure SI8: Low temperature NMR of **4** in 1:1 THF/*d*$_6$-benzene in the presence of 0.2 M $NaPF_6$. Top: ^1H-NMR. Bottom: $^{31}P\{^1H\}$-NMR.

For CV characterization, a 5 mM solution of **1** in 0.2 M $NaPF_6$ 2:1 THF/DFB was prepared and a CV recorded. Then a slight excess of $NaHBEt_3$ was added (6 mM). At 9 mM of $NaHBEt_3$, some dearomatized complex is also formed intermittently (Figure SI9).

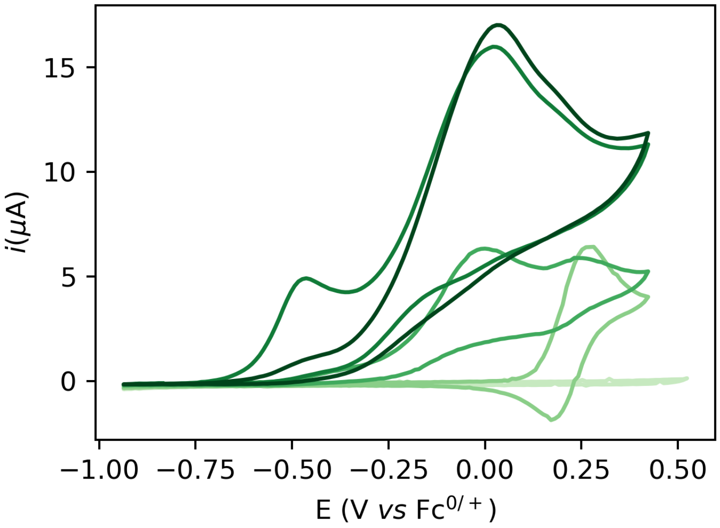

Figure SI9: From light to dark green: blank (0.2 M$NaPF_6$ in 2:1 THF/DFB, 0.1 V/s, 1 mm GC-electrode), 5 mM **1**, 5 mM **1** and 6 mM $NaHBEt_3$, 5 mM **1** and 9 mM $NaHBEt_3$ and 5 mM **1** and 9 mM $NaHBEt_3$ after 20 mn.

3.2. Characterization of 2 in 0.2 M $NaPF_6$ (2:1, THF/DFB)

In the glovebox, 15 mg (0.031 mmol) of **1** were reacted with 4 mg (0.035 mmol) of KO^tBu in 1.5 mL THF. After 2 h of stirring, the solvent was removed under reduced pressured and the crude was extracted with d_6-benzene, filtered over celite and NMR were recorded to confirm formation of **2**. The d_6-benzene solution was frozen at – 30°C and the solvent removed by sublimation under reduced pressure. The solid was then extracted with the electrolyte (0.2 M $NaPF_6$ in 2:1 THF/DFB) and a CV measure immediately. A half-wave potential of -0.45 V vs Fc was determined.

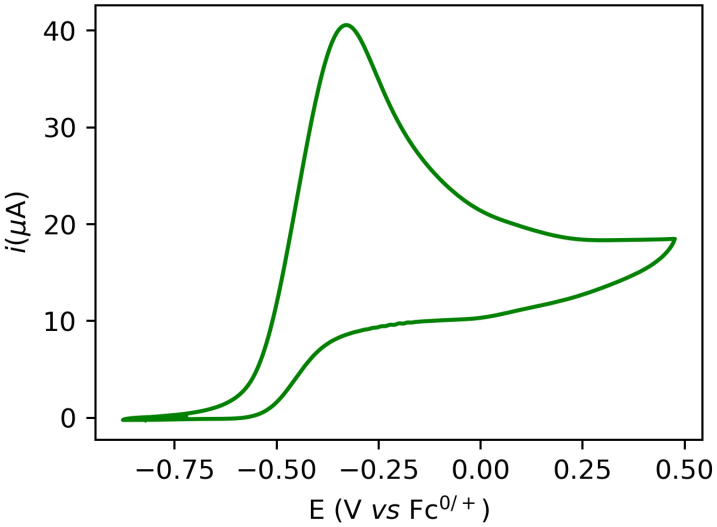

Figure SI10: CV of freshly synthesized **2** (roughly 10 mM) in 0.2 M$NaPF_6$ in 2:1 THF/DFB (0.1 V/s, 3 mm GC-electrode).

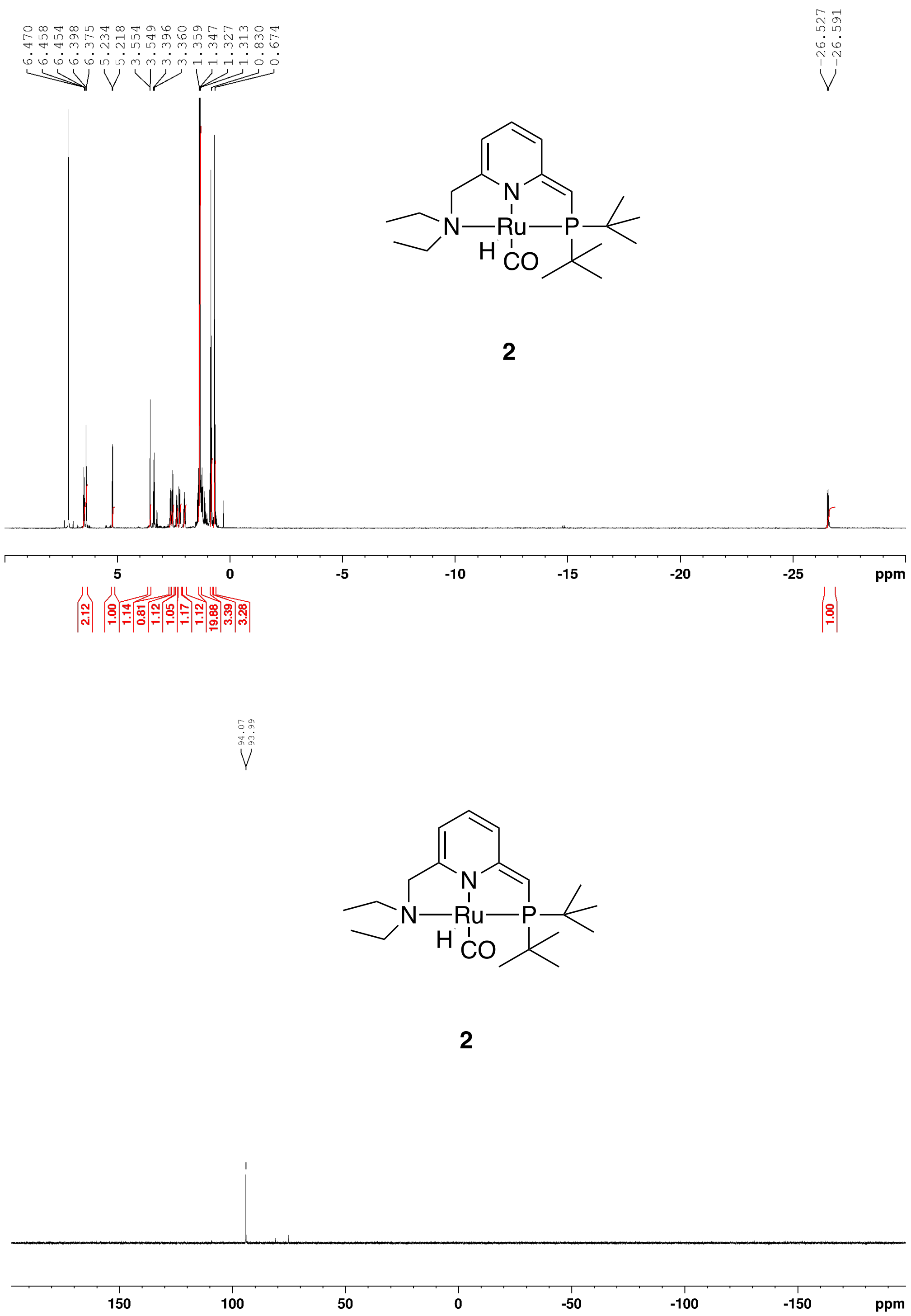

Figure SI11: ^{1}H (top) and ^{31}P{^{1}H} (bottom) NMR of **2** in *d*$_6$-benzene

3.3. Characterization of 3 in 0.2 M NaPF$_6$ (2:1, THF/DFB)

In a J-Young NMR tube, 4 mg (0.009 mmol) of **2** were dissolved 500 μL *d*$_6$-benzene and an excess 10 μL (0.17 mmol) ethanol were added. The reaction was monitored by ^{1}H- and ^{31}P{^{1}H}-NMR and formation of **3** was confirmed. As **3** is not stable under vacuum, the 500 μL solution was added to 2.5 mL of 2:1 THF/DFB with NaPF$_6$ to overall yield a 0.2 M NaPF$_6$ solution. A CV was recorded immediately afterwards. A half-wave potential of roughly -0.1 V vs Fc was measured.

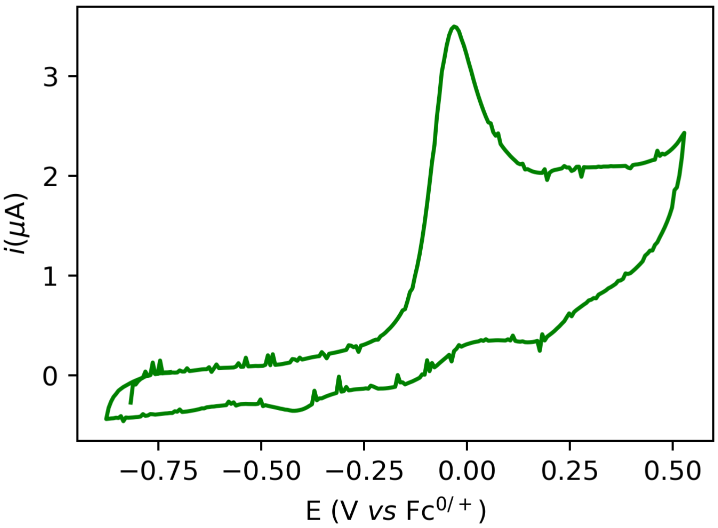

Figure SI12: CV of freshly synthesized **3** (roughly 3 mM) in 0.2 MNaPF$_6$ in a mixture of 0.5 mL *d$_6$*-benzene and 2.5 mL 2:1 THF/DFB (0.1 V/s, 3 mm GC-electrode).

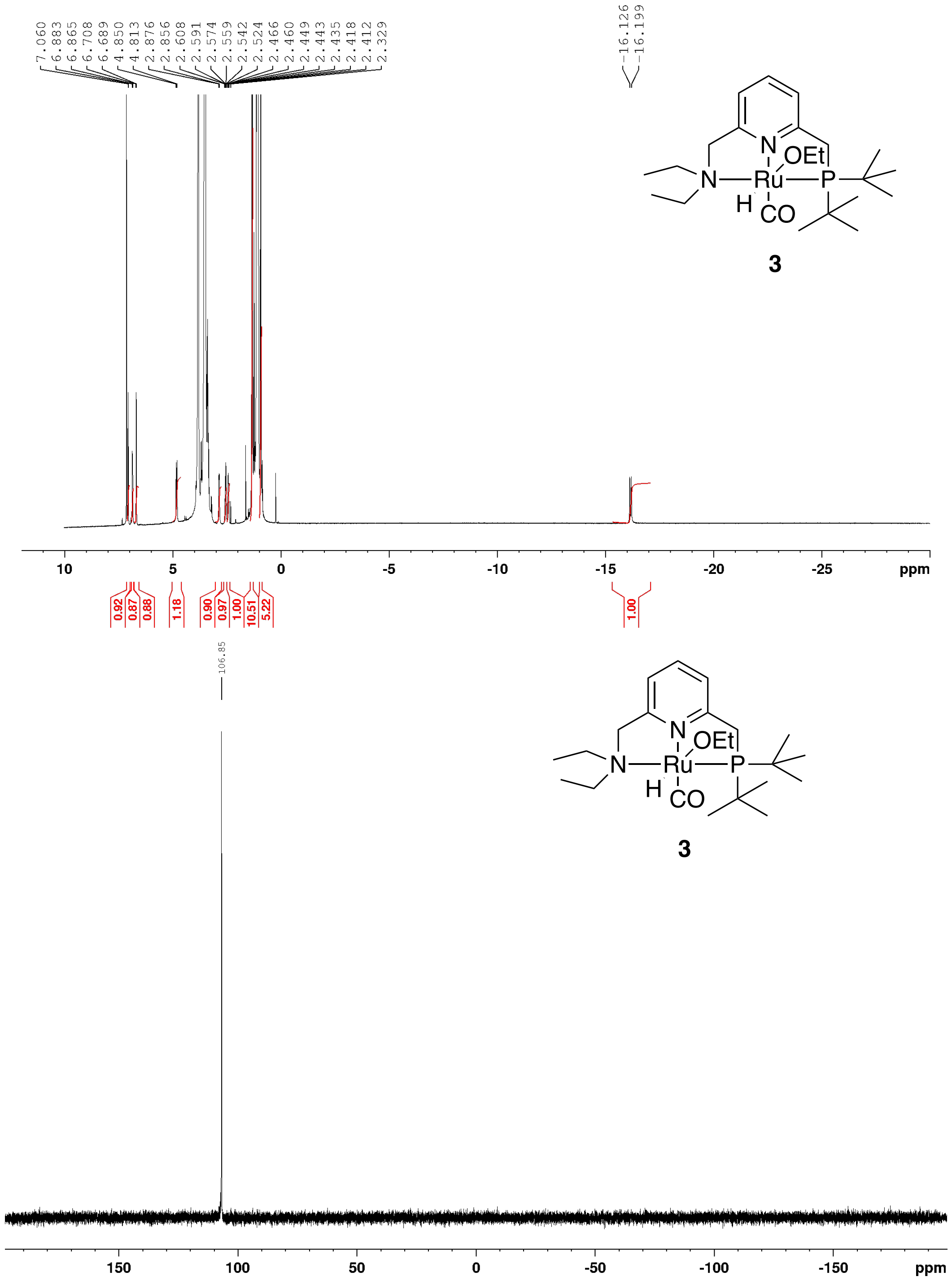

Figure SI13: ^{1}H (top) and $^{31}P\{^{1}H\}$ (bottom) NMR of **3** in d_6-benzene

4. Controlled potential electrolysis (CPE)

4.1. General

CPE were run in the same home-made 3 mL cell used for CV studies. The cell is placed in a water bath thermostated to 25°C. The working compartment is comprised of 3 mL of 0.1 M electrolyte (NaOEt or LiOH) in degassed and dried ethanol (stored over 4Å molecular sieves). The counter electrode (Pt-mesh) is immersed into 0.1 M $NaPF_6$ or $LiPF_6$ in ethanol and separated from the working solution by a porous ceramic frit. Prior to use, the counter electrode is rinsed and flame-annealed. The reference electrode for CPEs was a saturated SCE electrode, immersed into 0.1 M electrolyte in ethanol and separated from the working solution by a porous ceramic frit. The working electrode was a 2 cm^2 glassy carbon plate, which is washed, polished, sonicated, washed and dried prior to use. All CPE are run under an argon atmosphere (balloon). Pressure difference between counter and working electrode compartments are avoided using a cannula.

4.1. Reference spectra of acetate and ethyl acetate

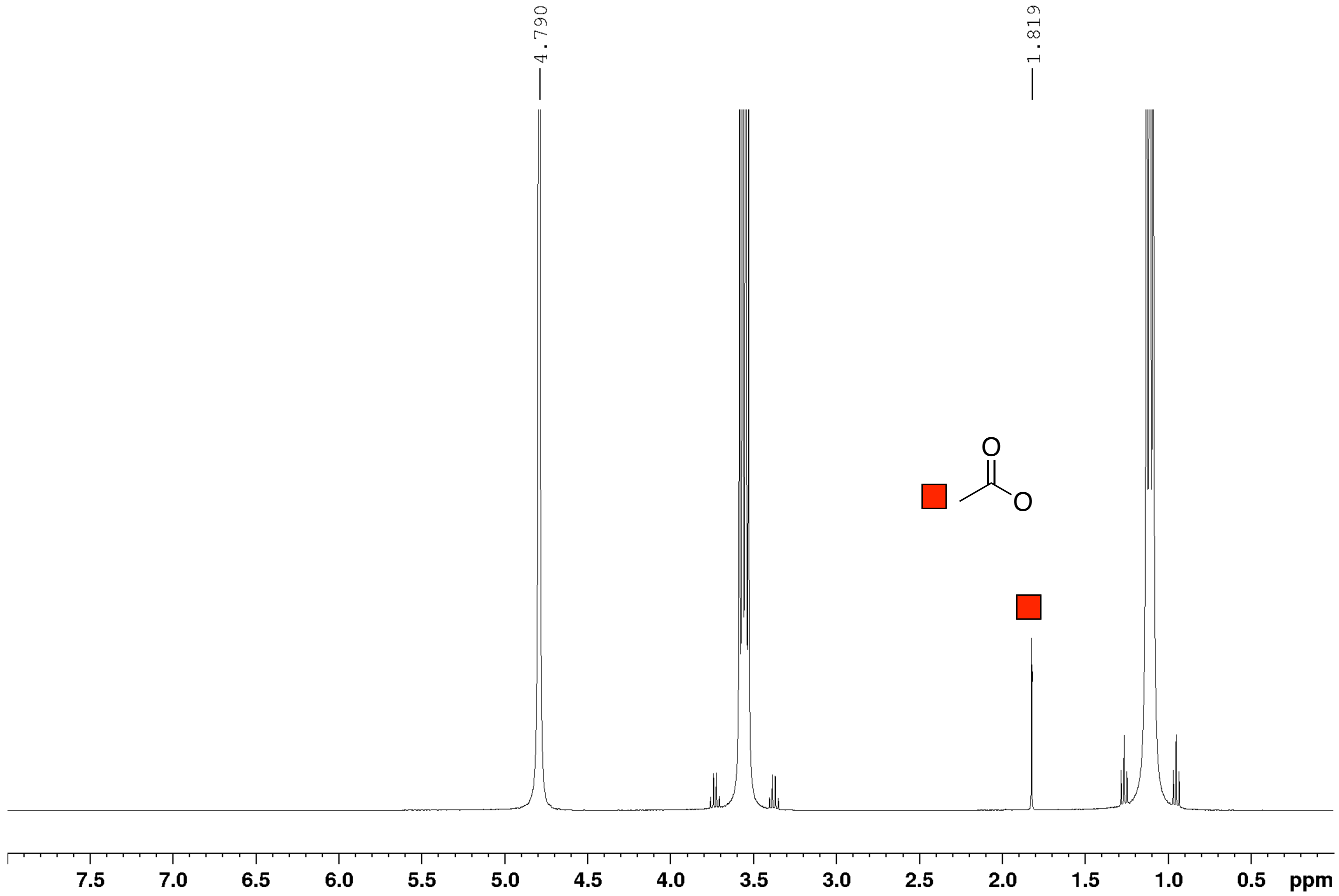

Figure SI14: ^{1}H of 3 mg potassium acetate in a 1:1 0.1 M LiOH in ethanol/D2O solution.

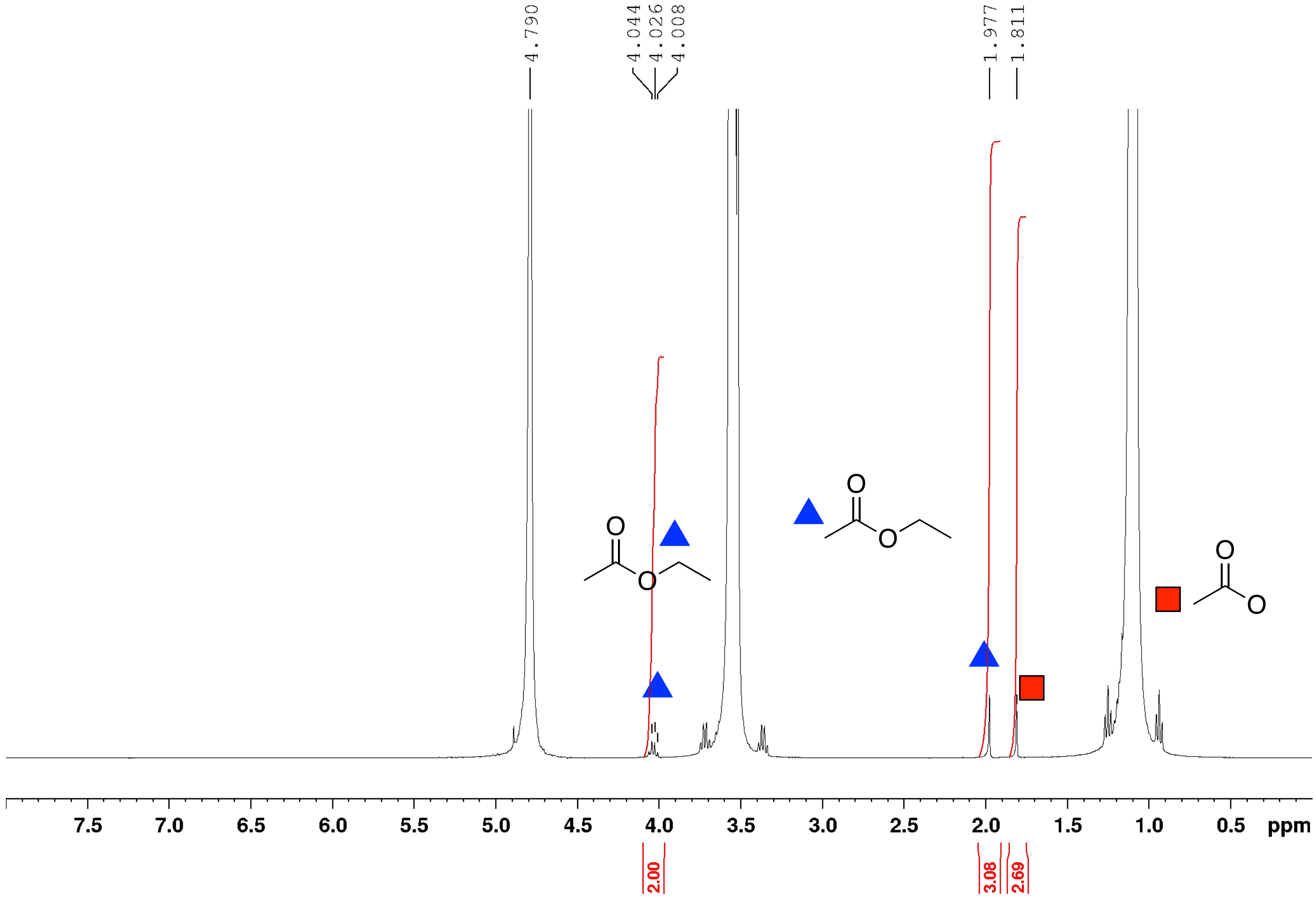

Figure SI15: ^{1}H of 3 μL ethyl acetate in a 500 μL 1:1 0.1 M LiOH in ethanol/D2O solution.

4.2. CPE in 0.1 M NaOEt in ethanol

Compared to LiOH (see below), reactions in NaOEt delivered lower currents (most likely due to catalyst degradation). Although peaks of acetate and ethyl acetate are present in the NMR spectrum, the low concentration did not allow for reliable quantification. In addition, the cation might play an important role as well, as already observed in numerous electrochemical systems.[2–8] We want to highlight though, that the presence of well-defined catalyst **1** is necessary and the role of Li$^+$ alone not sufficient to obtain selectivity for ethyl acetate and high TONs, as shown by blank experiments (see below). Nevertheless the roughly 15 % background activity for acetate production from the glassy carbon electrode should be noted.

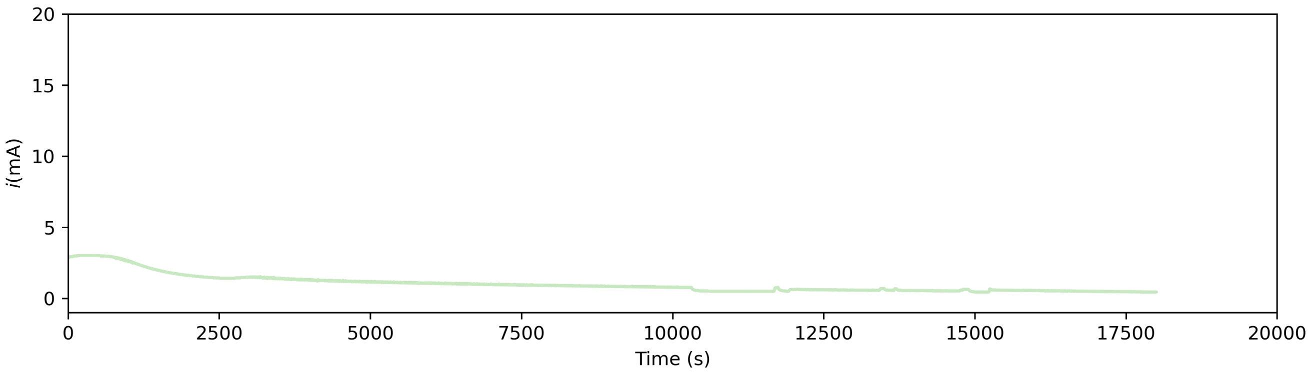

Figure SI16: CPE at 0 V vs Fc of 0.1 M NaOEt in ethanol with 1 mM **1**. Charge passed: 18.5 C.

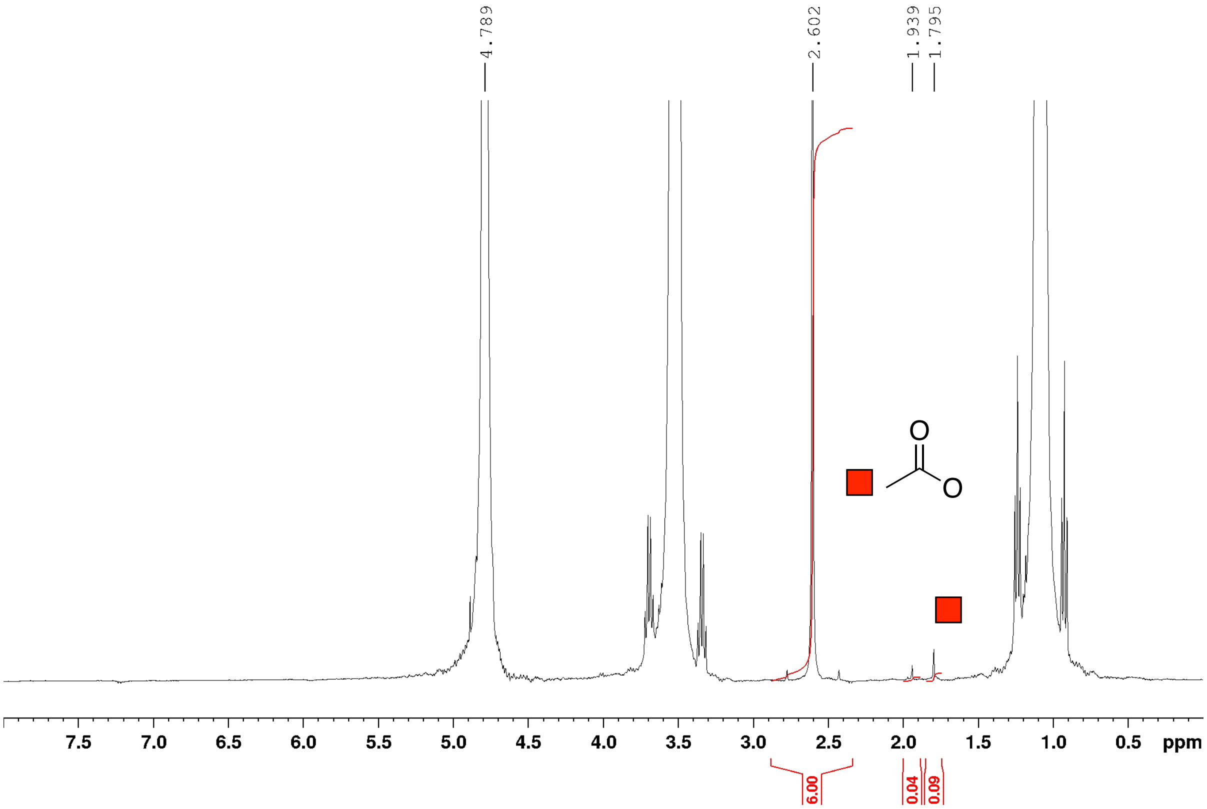

Figure SI17: ^{1}H of a 1:1 electrolyte/D_2O solution after electrolysis at 0 V vs Fc with 1 mM **1** in 0.1 M NaOEt in ethanol with DMSO as internal standard (5 μL).

4.3. CPE in 0.1 M LiOH in ethanol

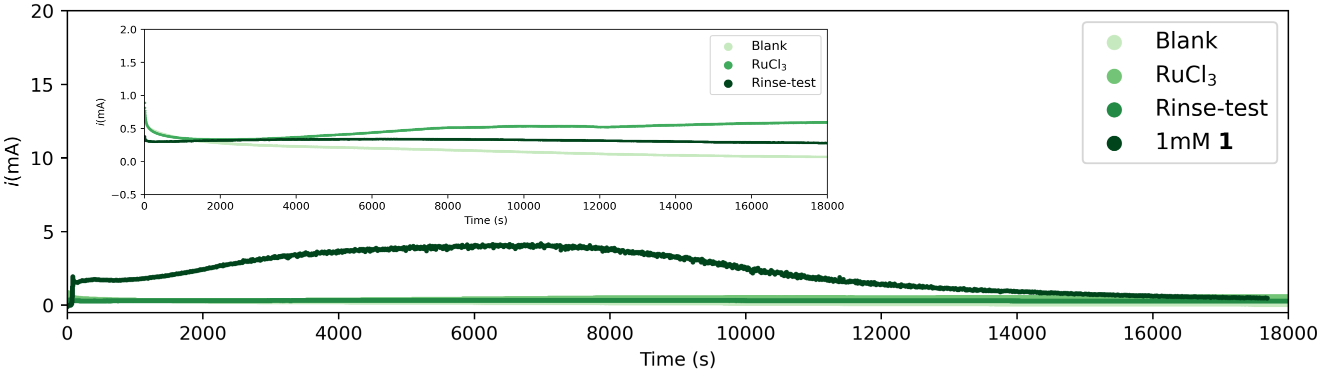

Figure SI18: CPE at 0 V vs Fc of 0.1 M LiOH in ethanol with no added catalysts, Ru-precursor ($RuCl_3$), an electrode after reaction (Rinse-test) and with 1 mM **1** (from light to dark green). Charge passed: 40.7 C with catalyst and 7.0 C without.

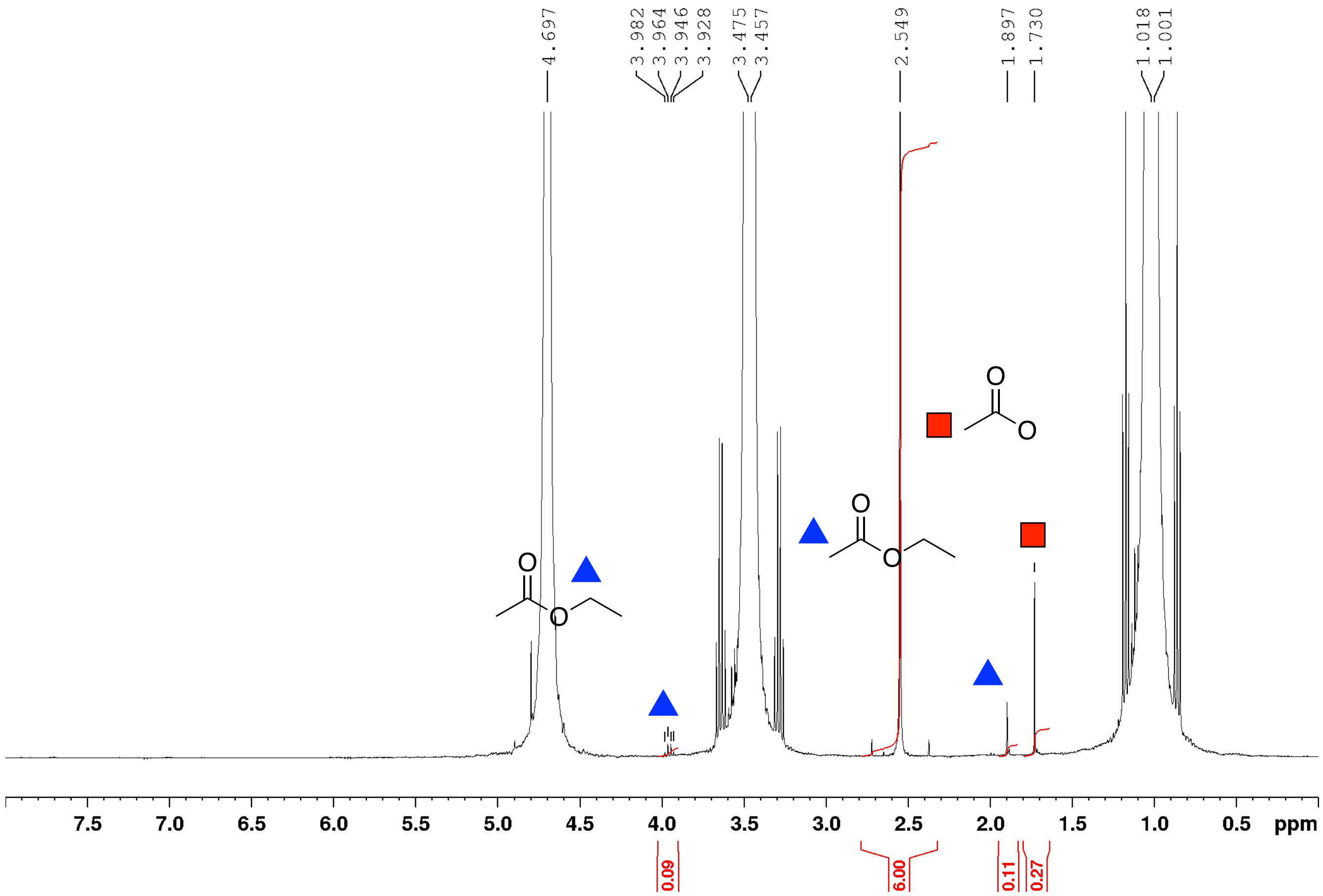

Figure SI19: ^{1}H of a 1:1 electrolyte/D_2O solution after electrolysis at 0 V vs Fc with 1 mM **1** in 0.1 M LiOH in ethanol with DMSO as internal standard (3 μL).

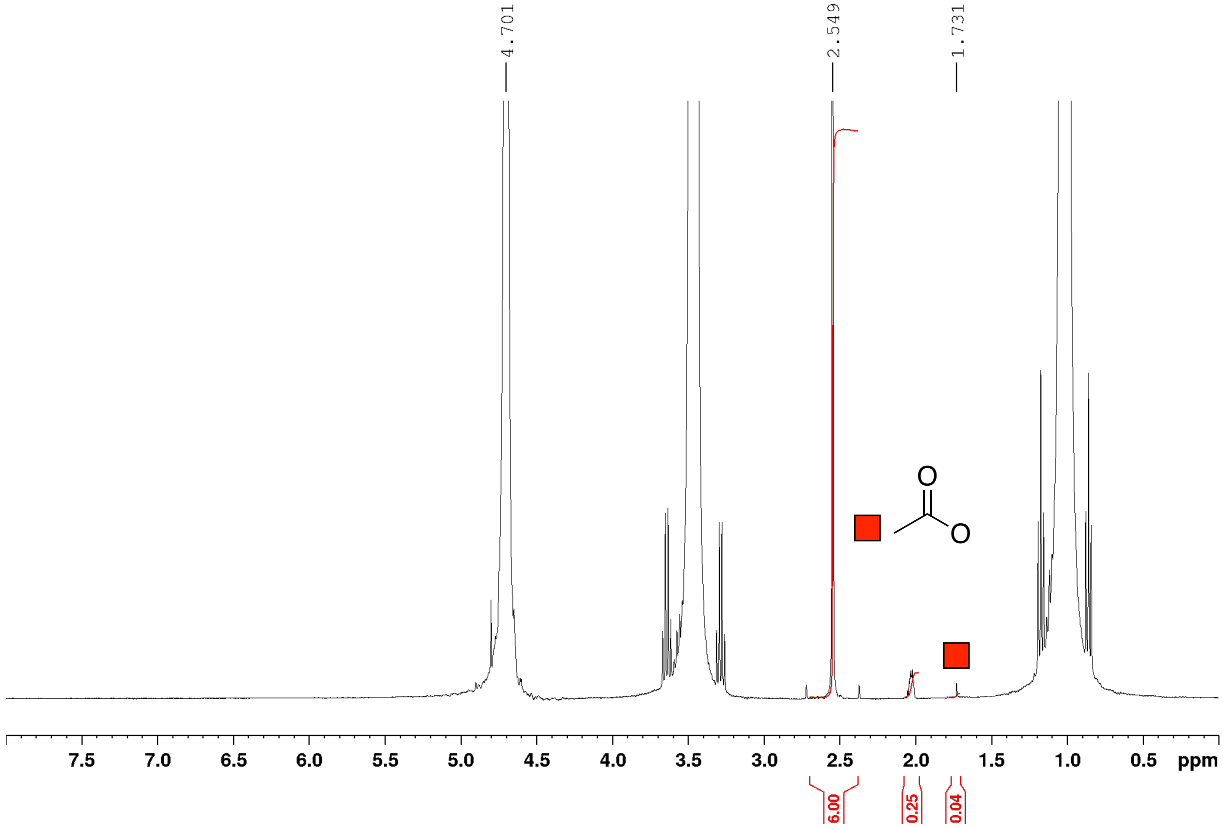

Figure SI20: ^{1}H of a 1:1 electrolyte/D_2O solution after electrolysis at 0 V vs Fc with no added catalyst in 0.1 M LiOH in ethanol with DMSO as internal standard (3 µL). Some acetonitrile impurities are present.

4.4. Blank experiment in the absence of applied potential

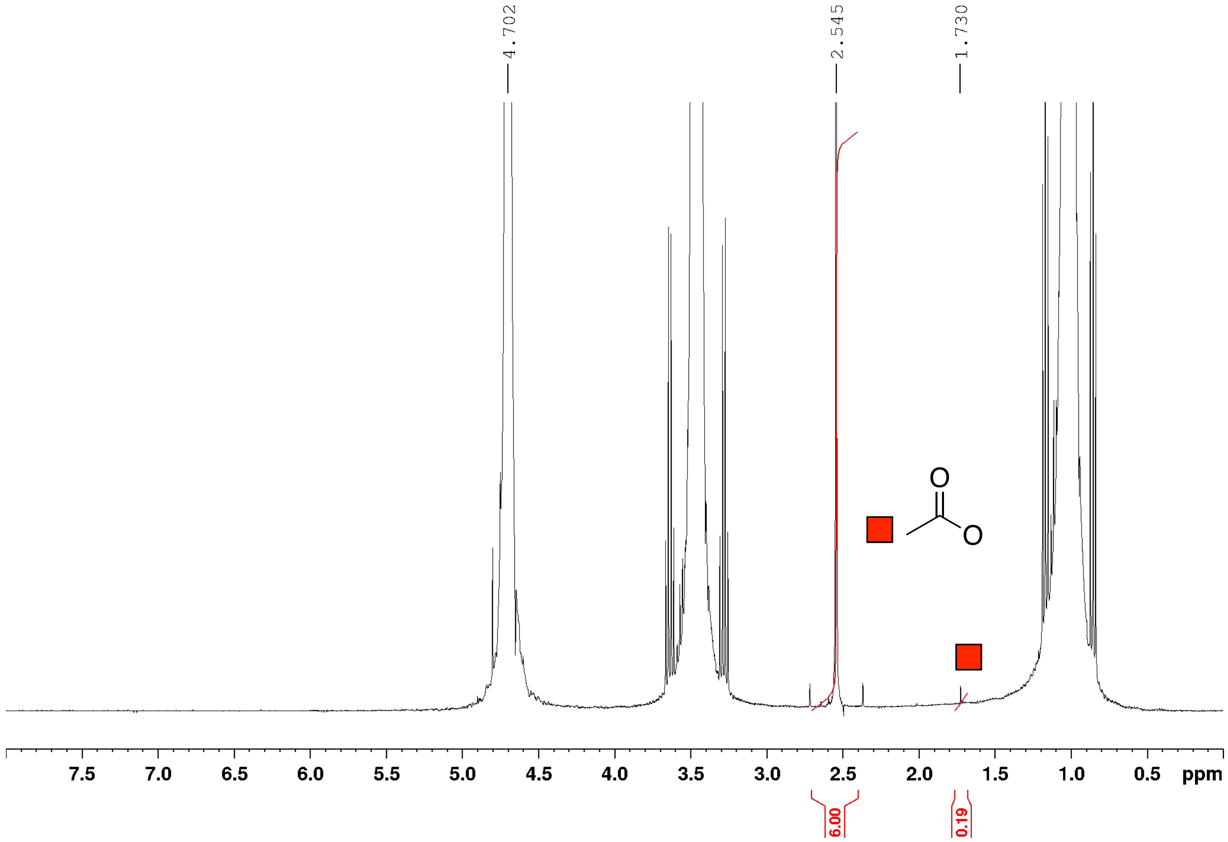

Figure SI21: ^{1}H of a 1:1 electrolyte/D_2O solution after 5 hr at 25°C in the presence of 1 mM of **1** in 0.1 M LiOH in ethanol with DMSO as internal standard (3 µL).

4.5. CPE with Ru-precursor

The employed Ru-PNN catalysts is not very stable under the employed reaction conditions, as highlighted by limited TON (<50 per 2 electrons) and the observed Ru-nanoparticle deposition on the electrode (see SI section 5 on SEM analysis). CPE using a simple Ru-precursor (1 mM $RuCl_3$) under standard conditions did not yield any formation of ethyl acetate.

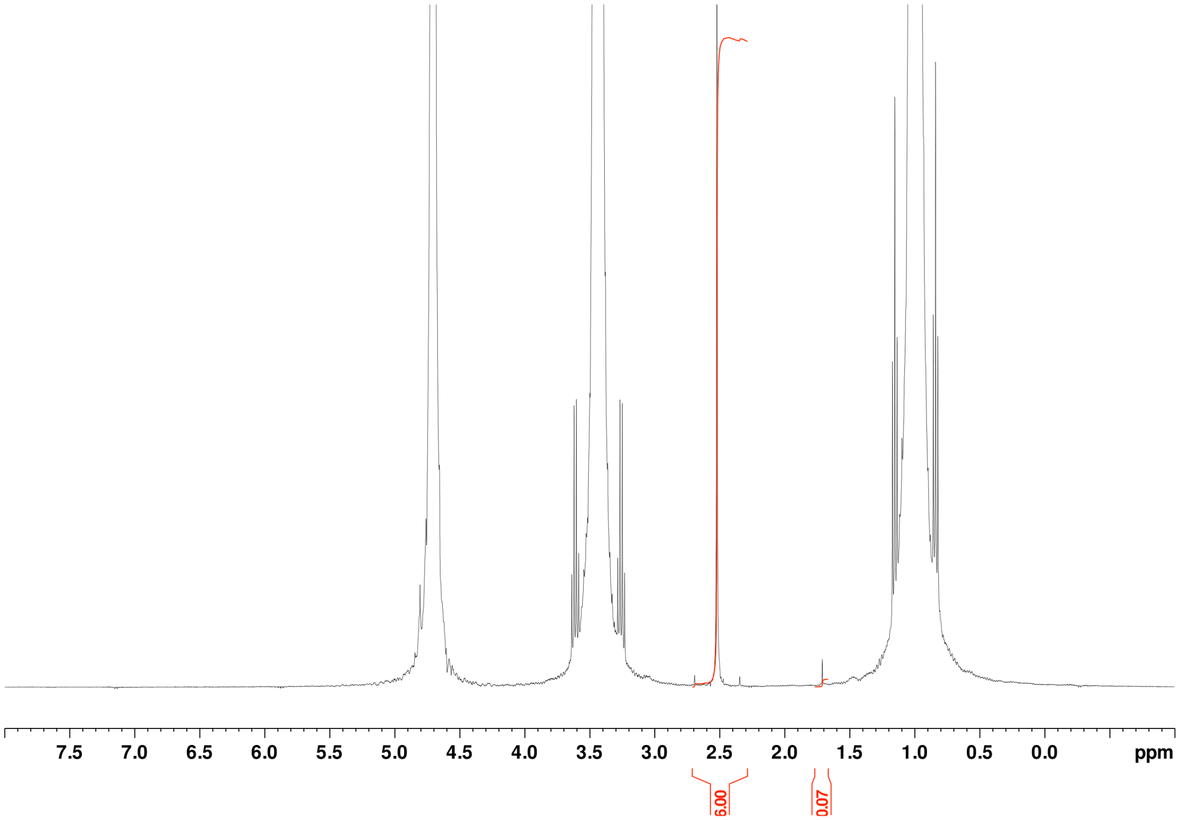

Figure SI22: ^{1}H of a 4:1 electrolyte/D_2O solution after 5 hr at 25°C in the presence of 1 mM of **$RuCl_3$** in 0.1 M LiOH in ethanol with DMSO as internal standard (3 μL).

4.6. CPE Rinse-test

After CPEs with the Ru-PNN complex, Ru-nanoparticles are found on the glassy carbon working electrode (see SI section 5 on SEM analysis). To exclude catalytic activity of the adsorbed nanoparticles, the electrode was carefully rinsed with milliQ water and used as a working electrode in a fresh solution of 0.1 M LiOH in ethanol. A CPE run under standard conditions with the nanoparticle decorated electrode, but in the absence of solubilized Ru-PNN complex showed no formation of ethyl acetate.

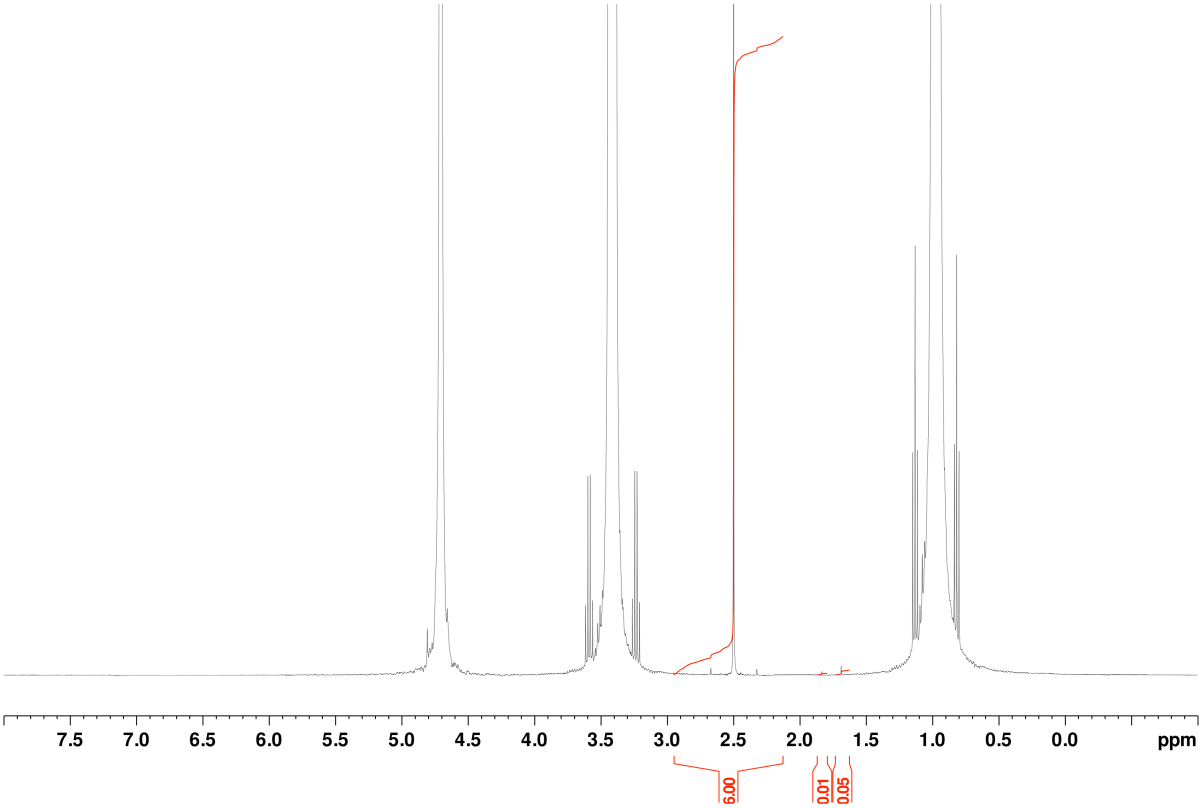

Figure SI23: ^{1}H of a 4:1 electrolyte/D_2O solution after electrolysis using a rinsed working electrode from a previous run for 5 hr at 25°C in 0.1 M LiOH in ethanol with DMSO as internal standard (3 μL) .

4.7. Verifying the homogeneous nature of the active species

As the catalyst is not stable under the electrochemical conditions and nano-particles are formed (see SEM analysis), we sought to test for the active species via classical methodologies, such as Hg-poisoning. In addition to its short-coming in homogeneous catalysis,[9,10] under oxidative conditions, applicability of the Hg-test limited in electrochemistry due to Hg-oxidation[11] at the potentials used for CPE in our system (see Figure SI24). We nevertheless ran Hg-poisoning CPE, with CVs run before and after CPE on a separate electrode to probe solution composition and activity. Although currents are lower than under usual CPE conditions, the CV response after CPE clearly shows an increase in catalytic current (Figure SI25). This is coherent with a new molecular species formed from **1** under CPE conditions and with the fact that current increase is less likely to stem from nanoparticles, although they are clearly present. After the Hg-poisoning CPE, the solution was evaporated to dryness and extracted with $CDCl_3$ to probe for molecular species. ^{1}H-NMR clearly shows the present of a hydride signal at roughly -4.5 ppm (Figure SI26). This chemical shift is extremely close to that of dihydride **4**, but ^{31}P{^{1}H}-NMR (66.9 ppm) indicates the formation of a different species (Figure SI26). Current efforts are devoted to fully characterizes this species and to understand catalyst speciation under preparative conditions.

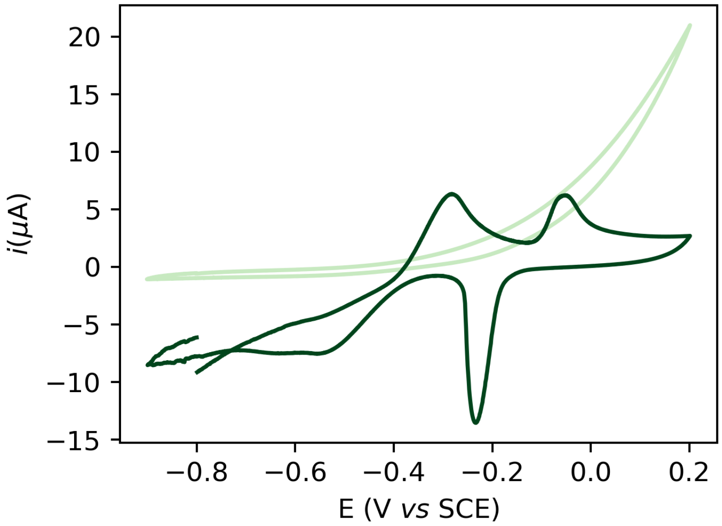

Figure SI24: CVs of 0.1M LiOH in ethanol at 0.1 V/s on a 1 mm Au-electrode (light green) and on a Hg-drop on the same Au-electrode (dark green), measured against SCE. Oxidation of Hg appears at significant lower potential compared to the working potential of CPE (roughly +0.38 V vs SCE).[12]

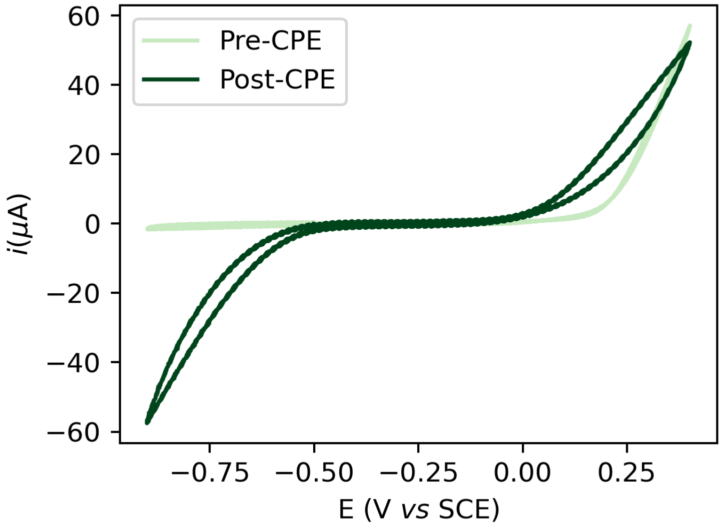

Figure SI25: CVs of 0.1M LiOH in ethanol, 1 mM **1** in the presence of a Hg-drop (roughly 0.2 mL) at 0.1 V/s on a separate 3 mm GC-electrode before (light green) and after (dark green) CPE. The current increase after CPE in the presence of Hg is indicative of a new molecular species responsible for increased catalytic activity.

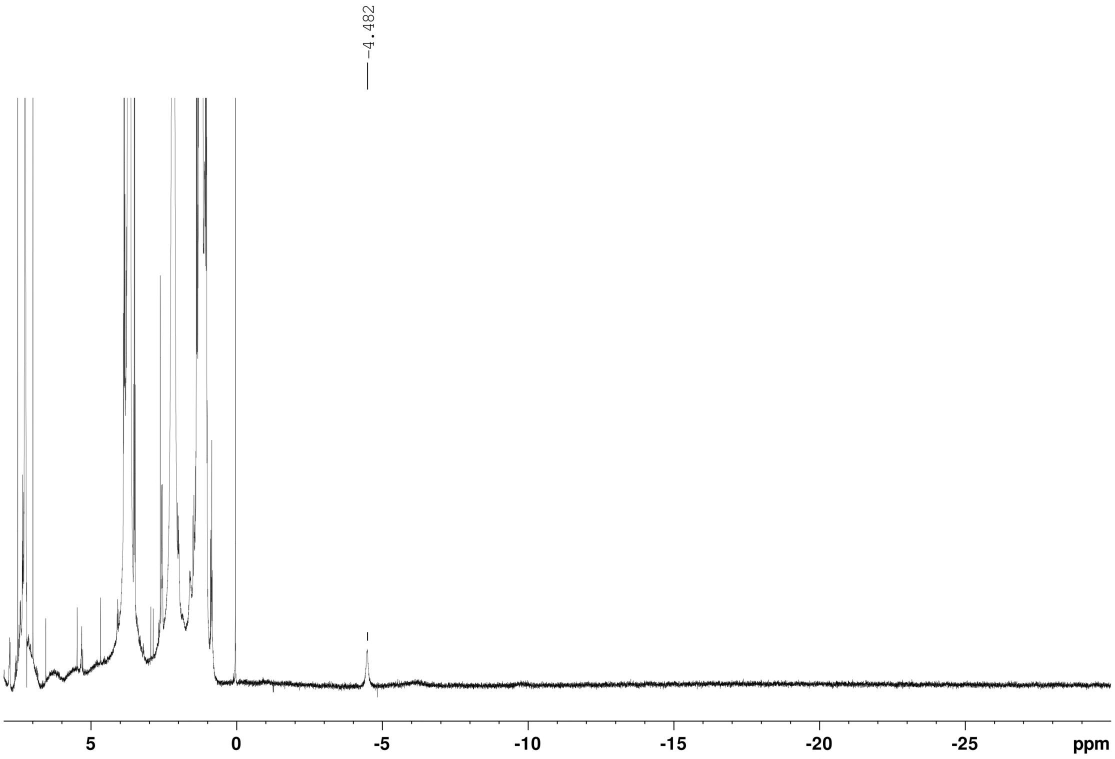

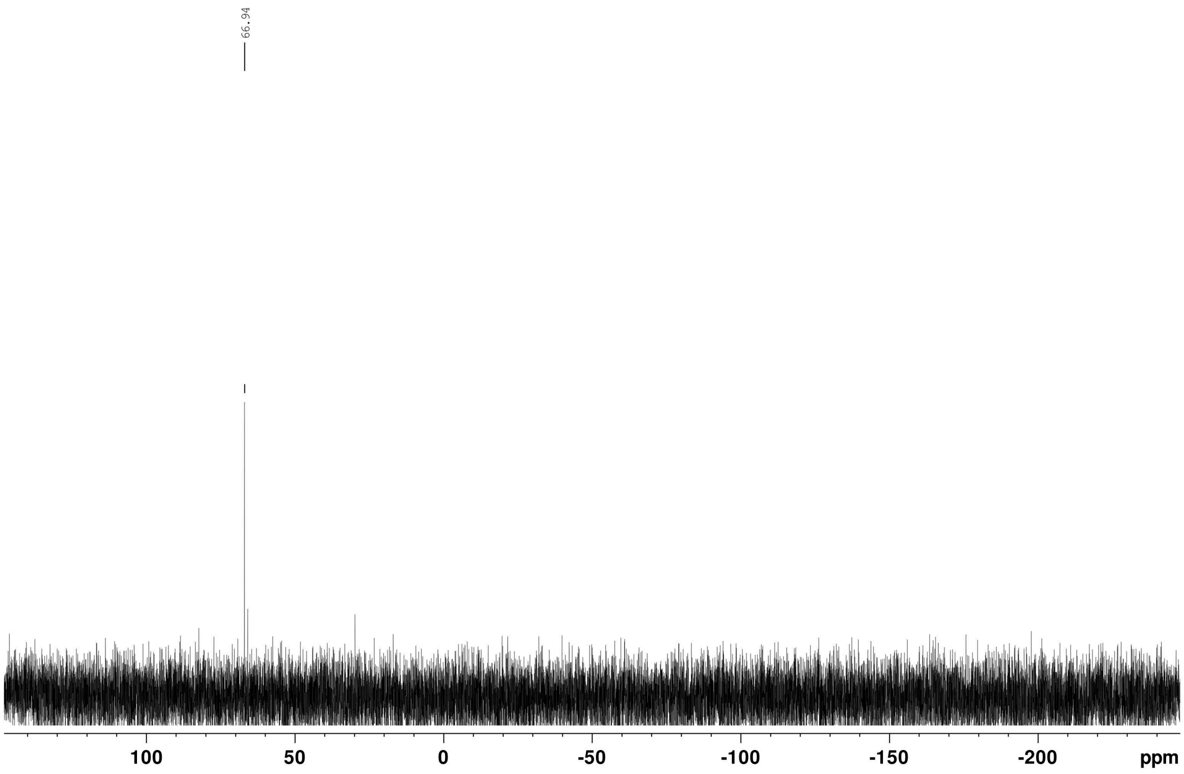

Figure SI26: ^{1}H (top) and ^{31}P{^{1}H} (bottom) NMR of the extract of the Hg-poisoning test post-CPE in $CDCl_3$.

5. SEM Analysis/Elemental Mapping

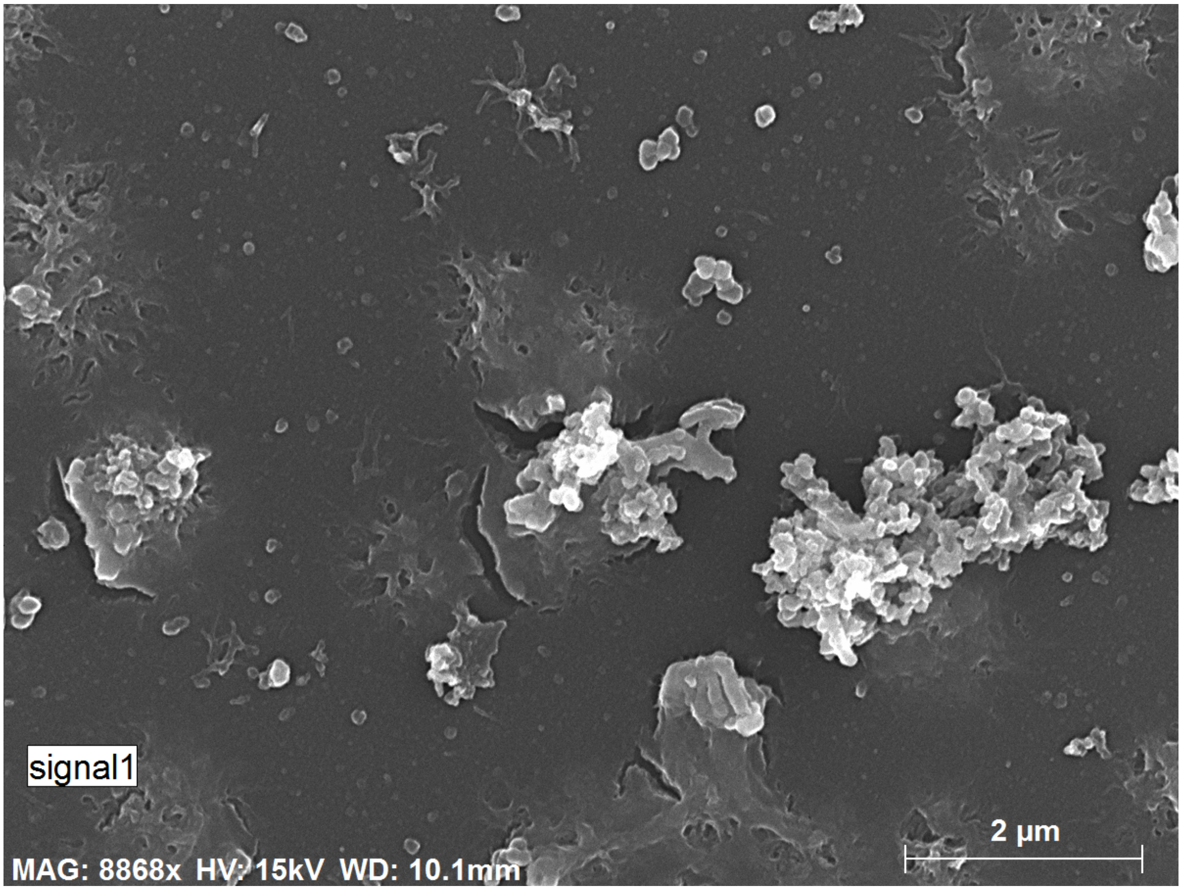

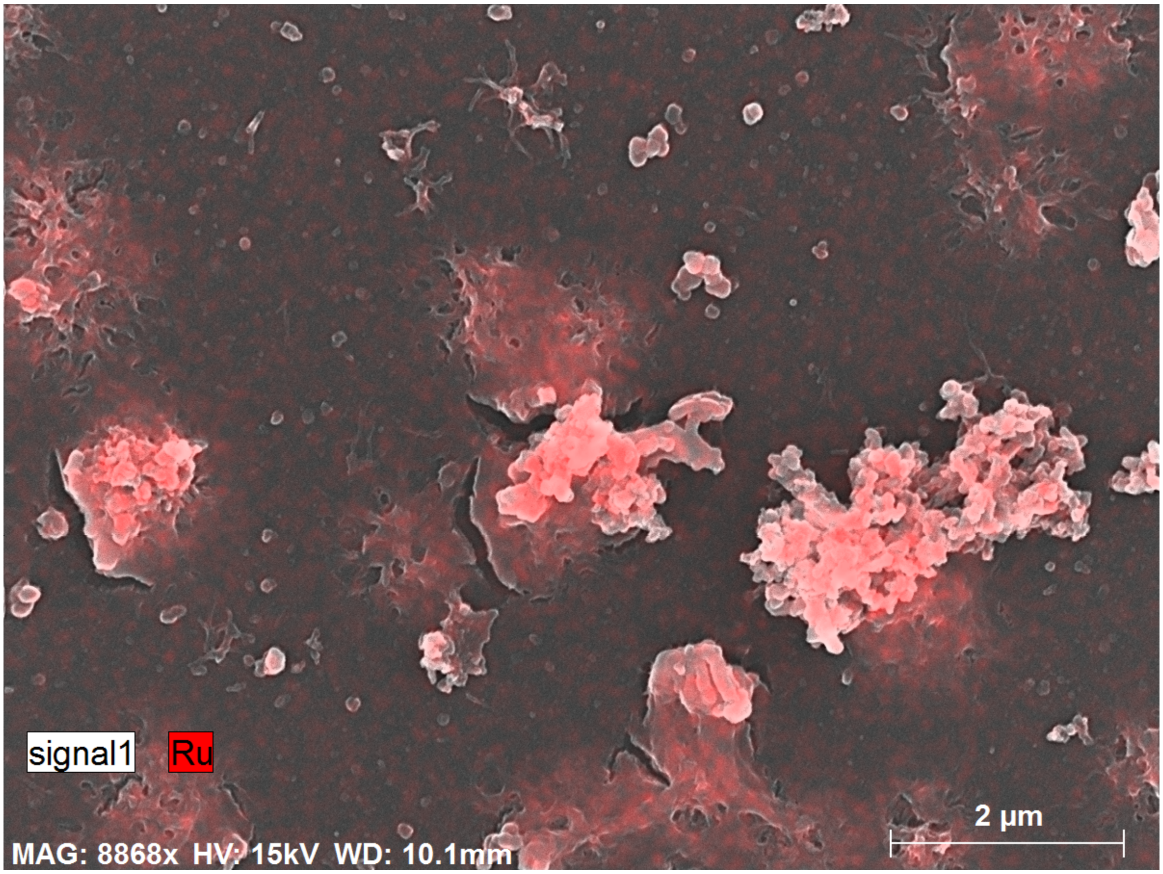

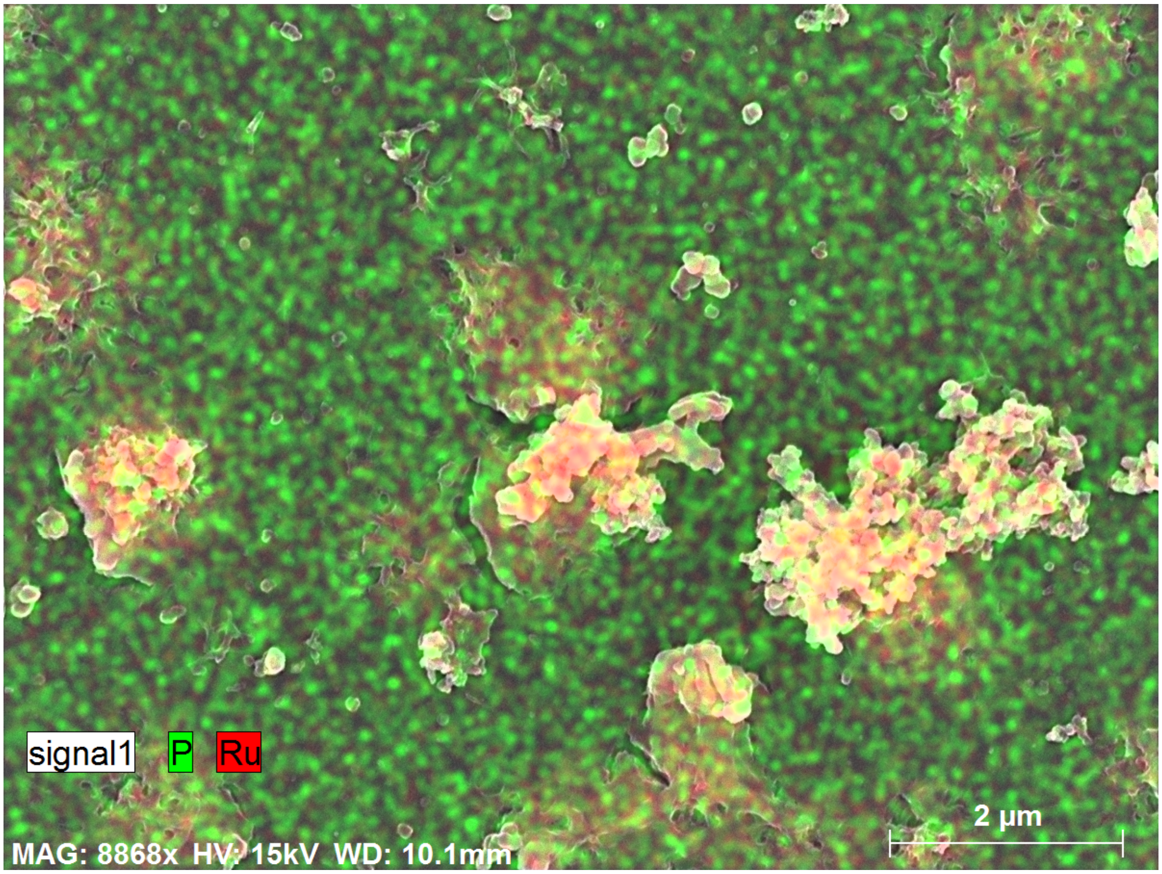

Figure SI27: SEM/Elemental mapping of a GC-plate post-CPE (standard conditions). From top to bottom: SEM image, Ru-channel, P-channel and overlap.

6. DFT Calculations

6.1. General

All geometries were optimized using the M06-L functional,[13] the def2-TZVP basis set[14] and W06 density fitting to increase computational efficiency,[15] as well as Grimme's empirical GD3 dispersion correction.[16] Frequency calculations at this level of theory confirmed stationary points and transition states and were used to compute thermodynamic properties at 388.15K, if not stated otherwise. Single point energies of the optimized structures were computed using the range-separated hybrid meta-GGA exchange-correlation functional ωB97M -V[17] including non-local correlation (VV10),[18,19] together with the triple-ζ def2-TZVPP basis set[14] and density fitting with the RIJCOSX formalism using the auxiliary basis sets def2/J[15] and def2-TZVPP/C[20] to speed up computational time. The choice of the ωB97M-V functional was rationalized given its excellent results in a recent benchmark study on transition metal reactions.[21] Gibbs Free Energies, unless otherwise stated, were computed by adding the Free Energy correction terms from the frequency calculations to the single point energies at the ωB97M-V/def2-TZVPP level of theory in solution (SMD, THF) according to:

$$G_{SMD}^{\omega BP97M-V} = E_{el/SMD}^{\omega BP97M-V} + corr_{freq/T}^{M06-L},$$

where

$$corr_{freq/T}^{M06-L}$$

is the thermal correction to the Gibbs Free Energy from the frequency calculation at temperature T.[22] All structures were optimized in solution (THF) using the integral equation formalism variant (IEFPCM) of the PCM model in the SMD variation of Truhlar and co-workers,[23] unless otherwise stated. Optimizations and frequency calculations were done using the Gaussian 16 software suite in the B.01 revision (Gaussian 16, Revision B.01, M. J. Frisch, G. W. Trucks, H. B. Schlegel, G. E. Scuseria, M. A. Robb, J. R. Cheeseman, G. Scalmani, V. Barone, G. A. Petersson, H. Nakatsuji, X. Li, M. Caricato, A. V. Marenich, J. Bloino, B. G. Janesko, R. Gomperts, B. Mennucci, H. P. Hratchian, J. V. Ortiz, A. F. Izmaylov, J. L. Sonnenberg, D. Williams-Young, F. Ding, F. Lipparini, F. Egidi, J. Goings, B. Peng, A. Petrone, T. Henderson, D. Ranasinghe, V. G. Zakrzewski, J. Gao, N. Rega, G. Zheng, W. Liang, M. Hada, M. Ehara, K. Toyota, R. Fukuda, J. Hasegawa, M. Ishida, T. Nakajima, Y. Honda, O. Kitao, H. Nakai, T. Vreven, K. Throssell, J. A. Montgomery, Jr., J. E. Peralta, F. Ogliaro, M. J. Bearpark, J. J. Heyd, E. N. Brothers, K. N. Kudin, V. N. Staroverov, T. A. Keith, R. Kobayashi, J. Normand, K. Raghavachari, A. P. Rendell, J. C. Burant, S. S. Iyengar, J. Tomasi, M. Cossi, J. M. Millam, M. Klene, C. Adamo, R. Cammi, J. W. Ochterski, R. L. Martin, K. Morokuma, O. Farkas, J. B. Foresman, and D. J. Fox, Gaussian, Inc., Wallingford CT, 2016). Single point energy calculations were performed using the ORCA software (4.1.1 release).[24] Molecular visualization was carried out using Chemcraft (https://www.chemcraftprog.com).

6.2. Redox potentials

Computed redox potentials[25] were obtained following the approach of Konezny and Batista.[26] In short, the oxidation potential of ruthenium bpy (Tris(2,2′-bipyridine)ruthenium(II) hexafluorophosphate) with respect to ferrocene was measured in 0.2 M $NaPF_6$ in 2:1 THF/DFB (+0.835 V).

The $G_{SMD}^{\omega BP97M-V}$ values for ruthenium bpy and its cation radical were obtained as described above in the presence of an explicit counterion molecule (PF_6). The redox potentials were then obtained by calculating ΔG of the isodesmic reaction of the ruthenium bpy couple with the couple of the different catalyst structures *via*:

$$E\left(V\ vs\ Fc^{0/+}\right) = \frac{\Delta G}{nF} + 0.835\ V \text{ with } n = 1 \text{ and } F = Faraday\ constant\ [kcal.V^{-1}mol^{-1}]$$

The experimental potentials are either the standard potentials in case of reversible waves or are approximated by the potential at half peak height.

6.3. pKa and BDFE values

The pK_a and BDFE values were obtained in a similar fashion to the redox potentials, i.e. using an isodesmic proton exchange reaction with a substrate of known acidity in THF, namely the protonated PNP complex **10**, which has an experimentally derived pK_a in THF of 20.7.[27] From the calculated ΔG of proton exchange between **10** and the complex of interest, the pK_a is derived (298 K). The BDFEs are then derived from the calculated pK_a and redox potentials according to:

$$BDFE = 1.364pK_a + nFE_{1/2} + \Delta G_{H^+/H}$$

, with $\Delta G_{H+/H}$ in THF of 59.9.[28]

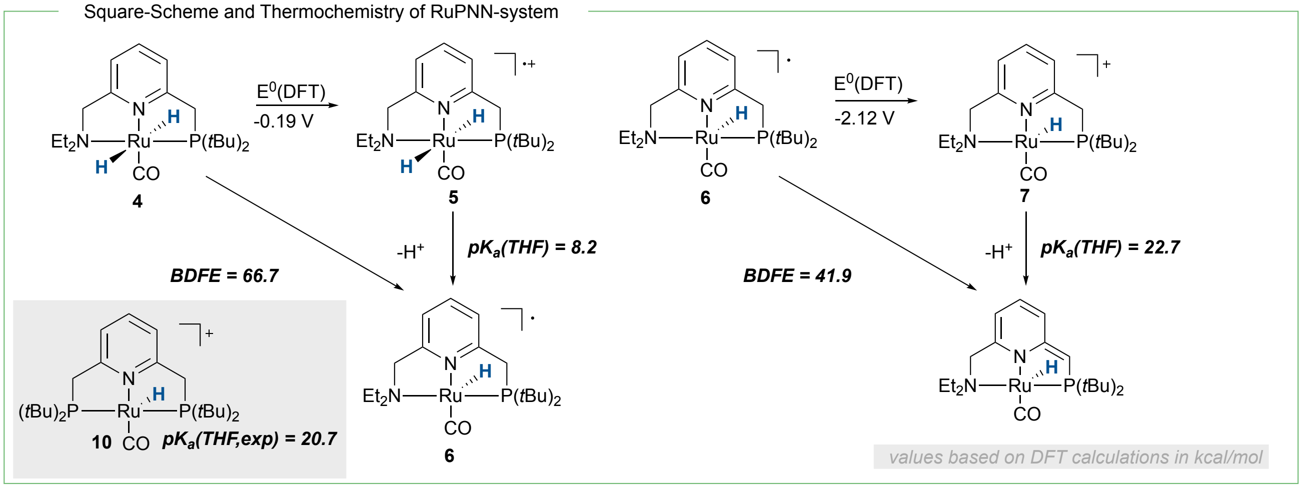

Figure SI28: Calculated thermochemical properties of the proton transfer, electron transfer events linking complex **4** with complex **2**, based on experimental data of complex **10**.

6.4. Calculation of PES and additional Transition States

For the calculations of energies and barriers of the neutral and cationic surface (Scheme 2 of the manuscript), as well as additional transition states (Figure SI24), the following procedure was applied. For the neutral surface, energies are calculated as highlighted above (Section 6.1) and reported against **2** (0.0 kcal/mol). For the cationic surface, the ΔG of one electron oxidations were calculated *via* $\Delta G = -nF\Delta E$ with $n = 1$ and $F = Faraday\ constant\ [kcal.V^{-1}mol^{-1}]$ and $\Delta E\left(V\ vs\ Fc^{0/+}\right) = E_{applied} - E_{1/2}$, with $E_{applied}$ being the applied bias (in this case 0 V vs Fc$^{+/0}$) and $E_{1/2}$ the oxidation potentials of the species derived from DFT-calculations. The ΔG for the electron transfer was then added to correct the cationic surface that were initially referenced versus **8**.

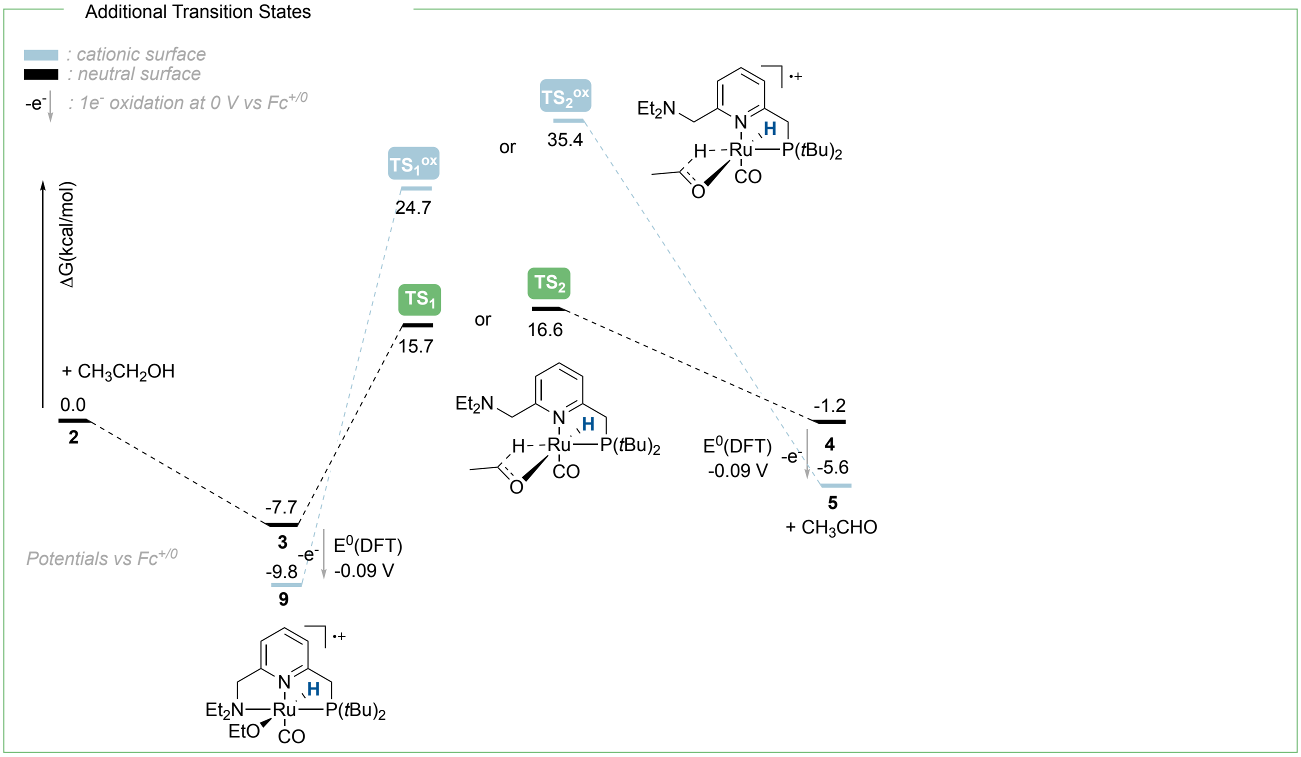

Figure SI29: Influence on ligand hemi-lability on hydride generating transition states in neutral and cationic form.

6.5. Computed structures and energies

All computed structures with their corresponding energies can be obtained free of charge at the following link on the ioChem-BD data repository: https://doi.org/10.19061/iochem-bd-6-117

7. References

1 D. Weingarth, A. Foelske-Schmitz, A. Wokaun and R. Kötz, *ECS Trans.*, 2013, **50**, 111.

2 T. Kumeda, H. Tajiri, O. Sakata, N. Hoshi and M. Nakamura, *Nat. Commun.*, 2018, **9**, 4378.

3 J. A. Rebstock, Q. Zhu and L. R. Baker, *Chem. Sci.*, 2022, **13**, 7634–7643.

4 L. Zhu, J. Du, S. Zuo and Z. Chen, *Inorg. Chem.*, 2016, **55**, 7135–7140.

5 K. Torbensen, C. Han, B. Boudy, N. von Wolff, C. Bertail, W. Braun and M. Robert, *Chem. – Eur. J.*, 2020, **26**, 3034–3038.

6 L. Droguet, M. Courty, O. Fontaine, J. M. Tarascon and A. Grimaud, *J. Electrochem. Soc.*, 2022, **169**, 070510.

7 V. Briega-Martos, F. J. Sarabia, V. Climent, E. Herrero and J. M. Feliu, *ACS Meas. Sci. Au*, 2021, **1**, 48–55.

8 D. A. Stevens and J. R. Dahn, *J. Electrochem. Soc.*, 2001, **148**, A803.

9 O. N. Gorunova, I. M. Novitskiy, Y. K. Grishin, I. P. Gloriozov, V. A. Roznyatovsky, V. N. Khrustalev, K. A. Kochetkov and V. V. Dunina, *Organometallics*, 2018, **37**, 2842–2858.

10 V. M. Chernyshev, A. V. Astakhov, I. E. Chikunov, R. V. Tyurin, D. B. Eremin, G. S. Ranny, V. N. Khrustalev and V. P. Ananikov, *ACS Catal.*, 2019, **9**, 2984–2995.

11 N. G. Yasri, A. K. Sundramoorthy, W.-J. Chang and S. Gunasekaran, *Front. Mater.*

12 V. V. Pavlishchuk and A. W. Addison, *Inorganica Chim. Acta*, 2000, **298**, 97–102.

13 Y. Zhao and D. G. Truhlar, *J. Chem. Phys.*, 2006, **125**, 194101.

14 F. Weigend and R. Ahlrichs, *Phys. Chem. Chem. Phys.*, 2005, **7**, 3297–3305.

15 F. Weigend, *Phys. Chem. Chem. Phys.*, 2006, **8**, 1057–1065.

16 S. Grimme, J. Antony, S. Ehrlich and H. Krieg, *J. Chem. Phys.*, 2010, **132**, 154104.

17 N. Mardirossian and M. Head-Gordon, *J. Chem. Phys.*, 2016, **144**, 214110.

18 O. A. Vydrov and T. Van Voorhis, *J. Chem. Phys.*, 2010, **133**, 244103.

19 W. Hujo and S. Grimme, *J. Chem. Theory Comput.*, 2011, **7**, 3866–3871.

20 A. Hellweg, C. Hättig, S. Höfener and W. Klopper, *Theor. Chem. Acc.*, 2007, **117**, 587–597.

21 M. A. Iron and T. Janes, *J. Phys. Chem. A*, 2019, **123**, 3761–3781.

22 B. Mondal, F. Neese and S. Ye, *Inorg. Chem.*, 2015, **54**, 7192–7198.

23 A. V. Marenich, C. J. Cramer and D. G. Truhlar, *J. Phys. Chem. B*, 2009, **113**, 6378–6396.

24 Software update: the ORCA program system, version 4.0 - Neese - 2018 - WIREs Computational Molecular Science - Wiley Online Library, https://wires.onlinelibrary.wiley.com/doi/full/10.1002/wcms.1327, (accessed October 20, 2021).

25 A. V. Marenich, J. Ho, M. L. Coote, C. J. Cramer and D. G. Truhlar, *Phys. Chem. Chem. Phys.*, 2014, **16**, 15068–15106.

26 S. J. Konezny, M. D. Doherty, O. R. Luca, R. H. Crabtree, G. L. Soloveichik and V. S. Batista, *J. Phys. Chem. C*, 2012, **116**, 6349–6356.

27 C. L. Mathis, J. Geary, Y. Ardon, M. S. Reese, M. A. Philliber, R. T. VanderLinden and C. T. Saouma, *J. Am. Chem. Soc.*, 2019, **141**, 14317–14328.

28 R. G. Agarwal, S. C. Coste, B. D. Groff, A. M. Heuer, H. Noh, G. A. Parada, C. F. Wise, E. M. Nichols, J. J. Warren and J. M. Mayer, *Chem. Rev.*, 2022, **122**, 1–49.